POINT-OF-CARE ELECTROFLOTATION OF DISPERSED, LOW TOLERANCE PATHOGENS IMPROVES DETECTION RATES BY LOOP MEDIATED ISOTHERMAL AMPLIFICATION

A THESIS SUBMITTED TO THE GRADUATE DIVISION OF THE UNIVERSITY OF HAWAIʻI AT MĀNOA IN PARTIAL FULFILLMENT OF THE REQUIREMENTS FOR THE DEGREE OF

MASTER OF SCIENCE

IN

MOLECULAR BIOSCIENCES AND BIOENGINEERING

DECEMBER 2017

BY:

Lena M. Diaz

Thesis Committee:

Daniel Jenkins, Chairperson
Yong Li
Tamara McNealy

Keywords: agricultural diagnostics, field testing, food pathogens, sample preparation, molecular diagnostics, nucleic acid amplification

ACKNOWLEDGEMENTS

Foremost, I wish to thank my supervisor, Dr. D. Jenkins, for his help and advice during my period of research. I would also like to thank Dr. Y. Li and Dr. T. McNealy for many conversations useful to and extending beyond this research. I am indebted to Ryo Kubota, who served as my mentor, constantly helping me troubleshoot the small but critically important details in molecular biology. I also thank Roberto Rodriguez for his assistance in machining prototype parts and being readily available for assistance and questions regarding Solid Works. Finally, I would like to thank our intern Natalie Walter, who helped tremendously to develop and validate the LAMP primer set in Objective 1.

DEDICATION

To my greatest inspiration, offering ceaseless support; my father, who over the phone and across an ocean helped me overcome my deficiencies in computer programming. And to my loving mother, who offered endless encouragement while reminding me to get a good night's sleep.

Table of Contents

LIST OF FIGURES

LIST OF TABLES

LIST OF ABBREVIATIONS

Ag ..... elemental silver

Au ..... elemental gold

ATCC ..... American Type Culture Collection

B3 ..... backward outer primer

BIP ..... backwards inner primer

BPW ..... buffered peptone water

C ..... Celsius

CCP ..... carbon conductive paste

CFU/mL ..... colony forming units/ milliliter

Cl ..... chloride

CPs ..... conjugated polymers

Da ..... daltons

DC ..... direct current

dH_2O ..... distilled water

DI ..... de-ionized

DNA ..... deoxyribonucleic acid

EDS ..... energy dispersive X-ray spectroscopy

EF ..... electroflotation

EPS ..... extracellular polymeric substance

F3 ..... forward outer primer

FIP ..... forward inner primer

h ..... hours

HT ..... high turbulence

Hz .....hertz

K ..... potassium

KCl ..... potassium chloride

kHZ ..... kilohertz

LAMP .....loop mediated isothermal amplification

LB ..... backward loop primer

LF ..... forward loop primer

LT .....low turbulence

mA .....milliamperes

mA/mm^2 ..... milliamps/ $millimeter^2$

mm .....millimeter

min ..... minute

mL .....milliliter

MW .....molecular weight

Ni .....nickel

NI ..... non-instrumented

PCB .....printed circuit board

PCR .....polymerase chain reaction

PDMS ..... poly(dimethyl)siloxane

PEG .....polyethylene glycol

POC .....point-of-care

Pt .....elemental platinum

s .....seconds

SA ..... surface area

SEM .....scanning electron microscopy

Ti .....elemental titanium

wt% .....percent weight

ρ ..... electrical resistivity

1. ABSTRACT

Molecular diagnostic systems are becoming increasingly portable enabling rapid direct detection of pathogens in the field. However, trace contaminations of pathogens on food and in the environment remain notoriously difficult to detect, eluding the most sensitive molecular methods. For example gene-based assays typically test sample volumes of 1-5 μL, so that a single replicate of even a robust assay is statistically unlikely to detect pathogens at levels below 10^2-10^3 CFU/mL. To address the logistical requirements for successfully detecting pathogens dispersed on an ecological scale, we have developed a portable point-of-care (POC) sample preparation system using electroflotation (EF) to preferentially recover pathogenic organisms dispersed in hundreds of milliliters by concentrating samples into small (μL) assay formats. Electrolysis reactions, supported on custom designed platinum coated titanium electrodes, generate hydrogen and oxygen micro bubbles that impel and displace suspended cells into a recovered concentrate. Electrolysis conditions and durations were controlled with a custom AndroidOS application, with a system designed to concentrate cells suspended in 380 mL of phosphate buffer (0.1 M) sample into a small user defined concentrate volume in 30 minutes or less. To enhance viable cell recovery, variable concentrations of Pluronic-F68 (0.01, 0.1 g L^{-1}) and chitosan oligosaccharide (0.01, 0.1 g L^{-1}) were added to the sample media containing 10^2, 10^3 or 10^4 CFU/mL of *Escherichia coli (E. coli) 25922* to produce shear protected flocs. EF processes were varied to include 10, 15 and 20 minutes of sample concentration at high and low turbulence flotation conditions. Evaluation of detection limits was conducted with and without EF treatment in a standardized loop mediated isothermal amplification (LAMP) assay targeting a single-copy gene (glycerate kinase) in *E. coli* 25922. By this method reliable detection (~>95 %) of *E. coli 25922* by LAMP was achieved at concentrations

down to 10^2 CFU / mL, representing an improvement in the detection limit of 3 orders of magnitude relative to untreated control samples.

2. INTRODUCTION

2.1 General

Food borne diseases result in hundreds of thousands of cases of illness, thousands of hospitalizations, and hundreds of deaths in the United States annually (Scharff 2012). The most common food pathogens include *Clostridium perfringens, Salmonella enteritidas, Camplyobacter spp., Staphylococcus aureus,* and *Escherichia coli O157.* Federal regulations, like the FDA Food Safety Modernization Act of 2011 (111th Congress 2011) identify the current state of public health attributed to food safety as a serious burden, but believe outbreaks of contaminations can be prevented by implementing preventative controls and standards across the food supply chain. One key recommendation is that good sanitation practices be conducted with routine testing for pathogens on-site by rapid detection methods to provide real-time results in order to mitigate outbreaks from food borne illness. In the last two decades rapid diagnostics based on immunological interactions (Chandler et al. 2001), nucleic acid based assays (Martzy et al. 2017) and other biosensors (*i.e.* Lab-on-chip technology) (You et al. 2011) have been integrated into miniaturized portable hand-held technology enabling detection in 1 hour or less. While rapid detection technologies seem ideal for on-site testing, they lack sufficient sensitivity for direct point-of-care (POC) testing (Mandal et al. 2011). As a result, trace contaminations of pathogens on food and in the environment, remain notoriously difficult to detect in a timely fashion.

The limit of detection by rapid methods is generally above 10^3 CFU/g of food (Abdel-

Hamid et al. 1999; Taylor et al. 2009). For example, gene-based assays typically test sample volumes of 1-5 μL, so that a single replicate of even a robust assay is statistically unlikely to detect pathogens at levels below 10^3 CFU/mL. This limit exceeds regulatory levels for many high-consequence pathogens.

Sample preparation methods like enrichment and concentration of bacteria can provide sufficient target for amplification in gene based assays, however severely delay the sample-to result time and require a lab facility (Stevens and Jaykus 2004). While methods like centrifugation (Maron et al. 2006), filtration (Karim et al. 2008), and immunomagnetic separation (Fu et al. 2005) have the ability to rapidly concentrate bacteria from samples, these approaches are challenging to implement in field and even rudimentary labs.

In summary, practical application of point-of-care (POC) diagnostics in agriculture, environmental, and food industries is beset with fundamental challenges including: 1) complex environmental sample matrices with many compounds potentially inhibitory of molecular assay reactions (Stevens and Jaykus 2004) 2), physical limitations on direct detection limits, necessitating extensive sampling and/or time-consuming enrichment for meaningful results, (Mandal et al. 2011), and; 3) logistical requirements for successfully detecting organisms dispersed on an ecological scale- for example, how to process large (liters or hundreds of mL) samples into small (μL) assay formats without losing meaningful information (Thatcher 2015).

The development of portable technologies capable of producing high quality sample preparation is a crucial, but under-researched step to realizing *truly* real- time detection with portable biotechnology for POC-testing in food safety, water quality or agricultural applications (Stevens and Jaykus 2004). While portable molecular diagnostics have reached commercial

maturity, technologies to facilitate sample acquisition and processing for use with downstream molecular testing platforms remain underdeveloped.

2.2 Fundamentals of Electroflotation (EF)

Flotation is a process that collects, transports and separates solids from liquid by particle attachment to gaseous micro-bubbles commonly generated from dispersed air flotation including electroflotation (EF), or dissolved air flotation (DAF) technology. Historically, flotation technology has widespread industrial applications including harvesting algae (Kurniawati et al. 2014; Walls et al. 2014), removing pollutants in tanneries (Murugananthan et al. 2004), aerating bioreactors to cultivate plant, animal and microbial cells (Joshi et al. 1996; Chisti 2000; Garg et al. 2014; Walls et al. 2014), effluent wastewater treatments (Chen 2004), mineral processing (Kyzas and Matis 2014), and removal of textile dyes (Szpyrkowicz 2005). The interaction and attachment of a particle to a bubble is a dynamic and complex process commonly modeled following colloidal particle science characterizations including surface hydrophobicity (Nguyen and Evans 2002), surface tension (Walls et al. 2014), bubble-to-particle size ratio, hydrodynamic forces (Sharma et al. 2005) and degree of turbulence in fluid (Szpyrkowicz 2005). Once a bubble binds a particle, the particle-bubble aggregates, which are less dense than their surrounding suspension, rise to the surface of the media where the particle-bubble flocs are concentrated and removed.

While industrial gas sparging commonly generates bubbles of diameters ranging from 100-2000 μm, electrolytically produced bubbles are significantly smaller with reported (Montes-Atenas et al. 2010; Gonzales et al. 2012) diameters of 20-40 μm. Electroflotation is a promising method to separate particles 1- 200 μm as demonstrated in mineral processing where ultrafine particles (< 4 μm) have been removed (Gonzales et al. 2012; Alam and Shang 2016). Interestingly

microorganisms have been used to increase retention of mineral suspensions acting as flotation enhancers or flocculants by modifying the surface chemistry of minerals from hydrophilic to hydrophobic (Zita and Hermansson 1997) .

Microbial cells range in size from 0.5-5 μm. The surface of microbial cell membranes tend to be hydrophobic due to the prevalence of hydrocarbons, extracellular polymeric substances and lipopolysaccharides composing the cell membrane. (Jacobs et al. 2007) This results in preferential adsorption of bacterial cells onto bubbles (Walls et al. 2014).

3. HYPOTHESIS

I hypothesize that electroflotation, with appropriate chemical additives, can be used to concentrate and recover small concentrations ($<10^3$ CFU/ml) of bacterial pathogens from bulk aqueous samples to facilitate rapid, reliable detection using portable diagnostic technology.

4. OBJECTIVES

Objective 1: Design and fabrication of an experimental prototype electrolysis cell (Figure 1) to investigate the concentration and recovery of small quantities of dispersed microorganisms from large volume (hundreds of mL) samples using electroflotation.

Objective 2: Custom engineer a cost effective, planar, corrosion-resistant electrode array to stably support vigorous electrolysis reactions.

Objective 3: Design a LAMP assay detection model to evaluate the efficacy of electroflotation as a sample preparation step for improved bacterial detection.

Objective 4: Develop media formulations to increase aggregation of bacteria, protect their cell integrity from to shear stresses at the gas-liquid interface of bubbles, and enhance recovery of detectable material of bacterial origin.

5. BACKGROUND

5.1 Electrolysis

The principle of electroflotation is fundamentally centered around electrolysis of water to evolve oxygen ($O_{2(g)}$) and hydrogen ($H_{2(g)}$) gas microbubbles, respectively generated by electron transfer at anodic and cathodic electrode surfaces. When an electric potential is applied to a set of electrodes in contact with an electrolytic solution, net positive current travels from the anode (positive) to the cathode (negative). If potential exceeds the redox potential difference for a paired set of half-reactions, such as evolution of oxygen at the anode and hydrogen gas at the cathode, those reactions can result in electron transfer across the electrode / electrolyte interface:

Anodic reaction	$2H_2O_{(l)} \rightarrow 4e^- + 4H^+ + O_{2(g)}$		**Eq. (1)**
Cathodic reaction	$4e^- + 4H^+ \rightarrow 2H_{2(g)}$		**Eq. (2)**
Overall reaction	$2H_2O_{(l)} \rightarrow O_{2(g)} + 2H_{2(g)}$	$\Delta E^\circ = -1.23$ V	**Eq. (3)**

The anodic reaction (1) especially is often different from that shown above. For example, sometimes a sacrificial material such as aluminum or iron is used for the anode to generate trivalent ions to enhance flocculation of electrically stabilized particles or colloids (Gregory and Barany 2011). Anodic reactions may also result in undesirable corrosion and passivation of metal anodes, or generation of reactive chlorine species from chloride ions in solution (such as used for electrolytic chlorination; Zhao et al. 2017). Electrolytic charge transfer through the media is facilitated by ionized salts such as potassium phosphate while the electrodes provide a physical interface between the buffer and electrical circuit driving current. Buffering salts such as phosphate

also moderate bulk pH changes due to imbalances in the acid-base chemistries of the half-reactions, and local pH changes due around individual electrodes.

The realization of highly efficient water electrolysis depends on the interactions between process parameters including applied voltage (V), current (I), media pH and conductivity, spatial geometry and arrangement of electrodes, electrode material, surface wettability (Alam and Shang 2016) and electrical resistivity (ρ). Electrical resistivity attributed to gas bubbles, activation energies, mass transfer, circuit resistance or electrode erosion can largely hinder electrolysis reactions (Santos et al. 2013). The initiation and propagation of corrosion is a major concern during electrolysis and is an inextricably linked process between the previously mentioned parameters and environmental conditions. Electrode corrosion can result in physico-chemical changes in the material composition and morphology, resulting in impaired ability to support redox charge transfer across the electrode / electrolyte interface. As a result it is highly critical that electrodes be designed to be resistant to mechanical and chemical degradation (Santos et al. 2013). The electrode material durability largely determines the reproducibility and efficacy of the electroflotation cell. Therefore, the electrochemical properties of the electrodes must remain stable under changes in operating conditions *i.e.,* resistant to corrosion over a wide range of applied potentials (V) and current densities (A/m^2).

5.2 Printed Circuit Boards (PCB's)

The first iteration of electrodes used in the EF assembly were custom designed planar, gold electroplated arrays patterned on a custom printed circuit board (PCB) manufactured by OSH-Park (Lake Oswego, OR, USA). PCB's are widely used for electronic assemblies and applications including cell phones, computers, and microelectronics. PCB's support conductive electrical

pathways by chemically etching patterns onto copper sheets laminated on non-conductive substrates. OSH-Park uses a typical FR4 epoxy glass as their substrate material. While PCB's may not be commonly used to pattern electrodes, PCB's do offer some unique advantages like custom patterning, relatively low costs, and quick manufacturing.

PCB's can be manufactured with complex electrical pathways through multiple copper conductor layers (typically 2 or 4, but sometimes as many as 16 or more) stacked between layers the dielectric substrate, and interconnected by metallic plated "vias". After the initial printing and lamination of the layers to bind them together the through holes are drilled and electroplated with copper. Although copper is the most common material used in microelectronics, copper is highly susceptible to rapid corrosion oxygen-rich environments (Bui et al. 2010). Corrosion is an energetically favorable process converting metals from a high to low energy form (de Leon and Advincula 2015). Therefore, exposed copper remaining on the circuit board will oxidize and rapidly erode or form a non-conductive oxide layer. To ensure corrosion protection of PCB's, surface finishes are used to protect the copper vias by preventing the formation of a passive oxide, while also providing a solderable surface (Salahinejad et al. 2017). Common surface finishes including hot air solder leveling (HASL), immersion tin, and electroless nickel immersion gold (ENIG). In the final stages of manufacturing, OSH-Park applies an ENIG surface finish to PCB's. ENIG is a double layer metallic coating of 0.05 μm – 0.2 μm of gold over 3.04 μm – 6.09 μm of nickel ENIG has been rated as one of the superior finishes exhibited desirable electrochemical properties like improved electrical interconnections with high conductivity, and supporting high current densities (Bui et al. 2010). Inert metals like Au are resistant to corrosion, however the reliability of the Au layer to protect the substrate metals from corrosion largely depends on the thickness, porosity, quality finish and the environmental exposure conditions (Ballantyne; Bui et

al. 2010). Degradation of PCB metals due to corrosion remains a challenging issue in electronics despite advances in electroplating surface finishes. Ultimately, corrosion of the surface or substrate metals can result in undesirable shorts or discontinuities in the patterned circuits or complete PCB failure (Fu et al.; Salahinejad et al. 2017). It is notable that the conditions required for electrolysis (*i.e.,* long durations of applied potential across electrode arrays in media containing aqueous electrolytes) are extremely corrosive, such that even relatively "inert" metals like gold can readily be oxidized.

5.3 Corrosion Inhibiting Coatings

As previously mentioned, surface finishes are used to protect the mechanical properties of the underlying copper electrical traces from corrosion. However, under harsh conditions such as application of high potentials on electrodes submerged in an electrolyte solution, corrosion is aggressive even on an ENIG surface.

Recently protection of metals and alloys from corrosive environments by conjugated or conductive polymer coatings has been achieved, offering a new area of research for corrosion control methodologies. In 1977, polyaceteylene was doped with iodine to convert the electrically insulating polymer into a material that exhibited high electrical conductivity. The discovery and development of a new class of polymeric materials by doping electrically insulating materials to convert them into electrically conducting polymers (CP) won the Nobel prize in chemistry in 2000 (Zarras et al. 2003). Conjugated chains of CPs have repeating units of polymer backbones containing π-electron networks. There are two main types of doping: oxidative or p-doped where electrons from the backbone are removed resulting in cationic polymers and reductive or n-doped where electrons are added to the backbone resulting in anionic polymers (Angelopoulos 2001;

Zarras et al. 2003; Khosla 2012). The cations and anions formed from the doping of an electron donor or electron acceptor act as charge carriers transforming the material to be electrically conductive. Doping allows the loosely bound electrons to ”push” charge across the alternating double bonds of the conjugated polymer resulting in an electrical current through the polymer chain (Rohwerder and Michalik 2007; Percino, M. J. and Chapela 2013). Polyanilines, polypyrrole, polyheterocycles, and poly(phenylene-vinylene) are common classes of CPs and are applied to the surface metal either chemically or electrochemically.

Extensive research has been done on CPs and their application as corrosion inhibiting coatings. While CPs demonstrate potential to prevent corrosion on the EF systems PCB electrode arrays, the application and synthesis of the CPs require complex chemistry and electropolymerization techniques and often volatile materials that are not compatible where autoclaving or other methods are necessary to sterilize surfaces used in molecular diagnostic methods. Despite low manufacturing costs, complicated adhesion of CPs due to incomplete electropolymerization to the metal, and thermal instability result in poor corrosion protection (Breslin et al. 2005). Our lab previously (unpublished material) reduced the rate of corrosion of gold electrodes by applying a polypyrrole coating onto the surface, however the corrosion resistance only lasted 20-30 minutes. Taking into consideration the aforementioned complications, CPs were ruled out as viable corrosion inhibiting coatings for our application.

While extensive research was being conducted on CPs in the early 2000’s, parallel research was being conducted on electrically conductive pastes and adhesives composed of conducting fillers including carbon, gold and silver, polymer binders (pasting liquids), additives and carriers (Zhang et al. 2012). The principle of conductive pastes is similar to conductive polymers in that ultimately both provide a protective barrier to the electrodes, except the application and synthesis

of the conductive paste film to the substrate material is much simpler, reducing the quantity of processing steps. Conductive fillers are homogenously dispersed within the polymeric adhesive matrix to achieve high conductivity throughout the matrix (Švancara et al. 2009). Particle-particle contact of additive conductive fillers forms an electrical pathway throughout a normally electrically insulating material. The number and quality of particle-particle interactions determines the resistivity of the matrix and a critical composition for conduction is reached when current can reliably flow through any path in the matrix without reaching an electrically isolated "dead end" (Montemayor 2002). In contrast, conjugated or conductive polymers rely on electropolymerization to form alternating double and single bonds in the polymer chain enabling electron delocalization throughout the whole matrix (Percino, M. J. and Chapela 2013). In this research we use a screen printing method where the conductive pastes are patterned in various shapes and thicknesses in a single step to the planar substrate using a screen mask followed by a thermal curing step (Metters et al. 2012; Metters et al. 2013; Moscicki et al.).

5.3.1 Silver Filled Conductive Epoxy

Silver filled conductive epoxy is a two-part, silver filled, electrically conductive adhesive rated for superior toughness, and high bond strength to similar and dissimilar substrates. EP21TDCS has extremely low volume resistivity (10^{-3} ohm cm^{-1}). EP21TDCS does not contain any volatile solvents, which often require extreme curing procedures to eliminate from the compound's matrix.

While silver is not a common electrode material used to support electrolysis, we hypothesized that it's use might confer several distinct advantages in our electroflotation process. Silver / silver chloride (Ag/AgCl) electrodes are one of the most commonly used reference electrodes due to

their relatively low standard state redox potential, and highly reversible nature of the Ag/AgCl redox reaction. We hypothesized that hydrogen could be efficiently evolved at a silver cathode at low electrical potential, while any chloride ions present in the electrolyte could be sequestered on a silver anodic surface. By alternating the potential between two silver electrodes, these processes could potentially be sustained by periodically reversing the chloridation / corrosion on the anodized surfaces. The reversible silver / silver chloride redox reaction conducted at low anodic potentials could inhibit the formation of reactive chlorine species in chloride containing media, helping prevent oxidative damage and lysis of microbial cells.

Media solutions containing chloride are not uncommon in microbial culturing and enrichment processes, including Tris-EDTA and sodium chloride (Winslow, C.-E.A., 1931). The presence of chloride in solutions becomes problematic during electrolysis when a voltage potential greater than 0.81 volts is applied, which is the potential energy required to drive the reaction in water to form hypochlorite (OCl^-):

$$Cl_{2\,(g)} + 2e^- \leftrightarrow 2Cl^- \qquad E°= 1.35\ V \qquad \textbf{Eq. 4}$$

$$HClO + H^+ + 2e^- \leftrightarrow Cl^- + H_2O \qquad E°= 1.482\ V \qquad \textbf{Eq. 5}$$

$$ClO^- + H_2O + 2e^{-\ -} \leftrightarrow Cl^- + 2OH^- \qquad E°= 0.81\ V \qquad \textbf{Eq. 6}$$

The formation of hypochlorite decreases the pH of the solution. Hypochlorite is a potent oxidizer and can potentially oxidize or disinfect suspended cells (WHO, 2007). Mitigation of electrochemically generated reactive chlorine species is necessary to prevent cell lysis and death of viable target pathogens so that cells collected by EF are preserved in a more intact state to facilitate detection.

5.3.2 Carbon Conductive Paste (CCP)

Carbon conductive pastes (CCP) have become popular in electrochemistry and have been used for the fabrication of carbon paste electrodes, sensors and detectors. CCP is a mixture of graphite powder and binders including epoxy resins or pasting liquids most commonly in the form of a black baste. Binders are chemically inert, non-volatile and are high viscosity materials (Švancara, I., Vytřas, K.,2009). CCPs physical properties like resistivity can easily be modified depending on the desired application. For example, adding ionic binding materials or chemically active binders in specific proportions facilitates charge transfer through the material. CCP's exhibit phenomenally high conductivity and low ohmic resistance, despite containing electrically insulating binders like silicone or epoxy. The electrochemical processes that enable CCP's high conductivity are not well understood, but are mostly attributed to graphite, a conductive material that is highly resistant to corrosion. Wiping or wetting the top layer of the CCP after electrochemical activity can renew the surface instantaneously, which is an emphasized advantage of the material (Švancara, I., Vytřas, K., 2009).

5.3.3 Conductive Silicone

Conductive silicone is a rubber base with repeating units of poly(dimethyl-siloxane) (PDMS). The elastomer is generally a smooth black paste with a tightly controlled viscosity to assure complete fill-in around complicated contours and complex configurations. Conductive silicone can be filled with metals like silver, copper, or gold to achieve superior conductivity, however these fillers are expensive and also are susceptible to corrosion. Similarly to CCPs, the electrical conductivity can be achieved by filling or impregnating silicone matrices that normally

have a high electrical resistivity ($\rho = 6.3 \times 10^6$) (Halladay, D., Resnik 1963) with graphite to achieve a low resistivity, conductive material state.

PDMS is a popular material suitable for biological applications such as biofilm growth substrate, cell culture, and for the fabrication of microfluidic devices or next generation DNA sequencing where fluid flows with capillary action (C. Luo et al. 2006; Zhao et al. 2012; Halldorsson et al. 2015). Despite the low-cost fabrication of PDMS, applications that use electroosmotic flow to drive or pump fluids across or through PDMS devices, as seen in microfluidics, are challenged by the inherent hydrophobic surface properties of PDMS. The non-polar methyl groups on repeating units of $-O-Si(CH_3)_2-$ cause the surface of PDMS to exhibit hydrophobic properties with a water contact angle of 105°-120° (Bhattacharya et al. 2005; Almutairi et al. 2012). Relative to this research, a hydrophobic electrode surface will affect the physio-chemical parameters during electrolysis including bubble nucleation, growth and detachment from the surface. The amount of time a bubble occupies a domain on the electrode surface before detaching is regulated by the relative magnitude of surface energies at the gas/electrode and electrolyte/electrode interfaces and, therefore, gas bubbles stick longer and grow larger in size on hydrophobic surfaces (Bouazaze et al. 2006).

Given these challenges, extensive research has been done to develop surface treatments to improve the wetting characteristics of PDMS so that the surface is permanently modified to exhibit hydrophilic properties. PDMS surface treatments include chemical and physical techniques like removing uncured oligomers, monomer grafting (Hu et al. 2002), and doping PDMS with chemicals (Bodas and Khan-Malek 2006; Y. Luo et al. 2006). Among numerous methods of surface modification, extensive studies use oxygen plasma treatment of PDMS for its low cost, rapid and reliable application (Bhattacharya et al. 2005; Bhattacharya et al. 2007; Bodas and Khan-

Malek 2007; Almutairi et al. 2012; Hemmilä et al. 2012; HOFFMANN et al. 2012; Zhao et al. 2012). Exposure to oxygen (O_2) plasma treatment oxidizes the PDMS surface so that the exposed methyl groups on the repeating -O-Si$(CH_3)_2$- units are replaced with hydroxyl (-OH) polar groups to form hydrophilic functional silanol groups. Although the one-step O_2 plasma surface activation is highly effective, it is not stable over long periods of time resulting in hydrophobic restoration of the PDMS surface within hours to days. The instability of O_2 plasma treatment can be attributed to the migration of mobile low molecular weight, uncured polymers containing untreated non-polar siloxane groups rearranging towards the surface of the PDMS (Bhattacharya et al. 2005; Hemmilä et al. 2012). Therefore, grafting and tethering additional surface functional groups are necessary to make the hydrophilic modification permanent. Research has shown that grafting polyethylene-glycol (PEG) by physisorption can permanently attach terminal hydroxy groups onto longer chain hydrocarbons that maintain a much more stable orientation on the surface of O_2 plasma treated PDMS (Hemmilä et al. 2012) (Figure 1).

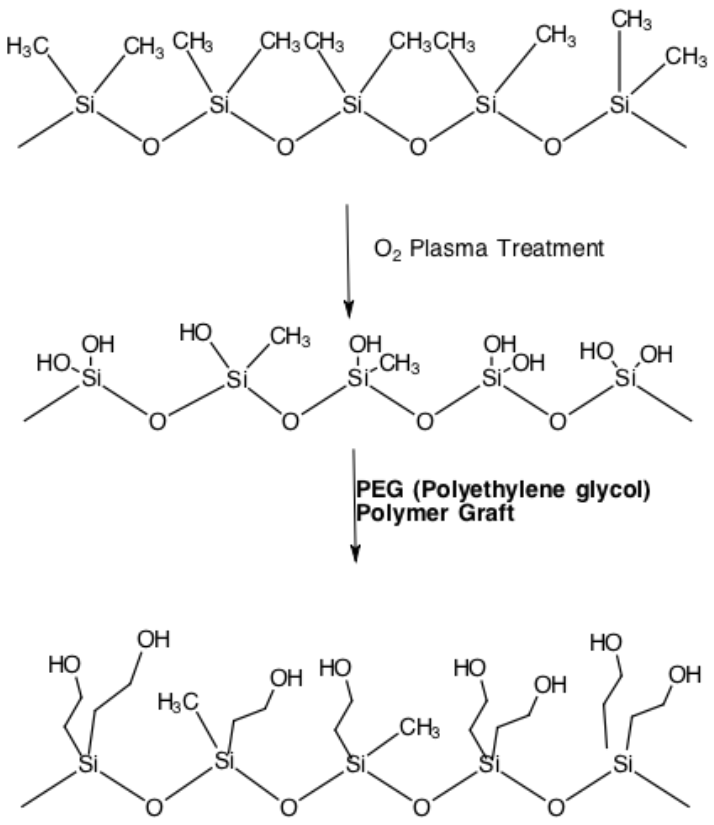

Figure 1. Mechanism PDMS hydrophobic to hydrophilic surface modification. O_2 plasma treatment followed by PEG grafting. Designed in Chem-Doodle software.

5.4 Platinum Coated Titanium Electrodes

In the last few decades the chlor-alkali industry has devoted much research to produce electrodes that are not disposable during water treatment and disinfecting processes. H. Beer used metals that remain conductive as oxides and also are robust against anodic polarization (Duby 1993). Progress in this industry has resulted in lowered manufacturing costs and custom design including patterning and cutting of metals. Commercial companies, like Qi Tin Xi in China who eventually manufactured our electrodes, are able to affordably manufacture prototype volumes of custom electrode designs. Titanium anodes coated with a 5-micron layer of platinum have high

anticorrosion resistance and are therefore not consumed or dissolved during electrolysis, have a long working life, and low operating voltage so that power consumption remains low.

5.5 Electroflotation Assisted Recovery by Chemical Additives

5.5.1 Flocculation by Chitosan

Flotation by microbubbles relies on the attachment of a particle to the bubble to form bubble –floc aggregates that rise to the surface of the media. Research on methods to concentrate dispersed microbes in a viable state using flotation is incredibly sparse, however methods used in wastewater treatment or processes involving stabilization and separation of dispersed systems can be applied so that flotation efficiency can be approved. As seen in sewage purification or ore refineries, aggregating particles prior to flotation can result in a substantial increase in particle quantity recovered (Lazarenko E.N., Baran A.A. 1986). Furthermore, harvesting microalgae and algal biomasses by flotation to use as biofuels has recently become a popular topic of investigation largely attributed to increased interest in alternative energy sources. For large-scale production of biofuels, significant research has reported air flotation as a competitive method to extract microalgae dispersed in suspensions by froth flotation (Garg et al. 2014), dispersed air flotation (Kurniawati et al. 2014) and less commonly, by electro-flotation (Ghernaout et al. 2015). Considering numerous applications of flotation of biological materials, flotation was optimized to achieve 99% recovery rates of *Chlorella sp.* (Zhou et al. 2016), bacterial suspensions including *E. coli* (Strand et al. 2002; Rinaudo 2006), and microalgae (Kurniawati et al. 2014) by adding cationic polyelectrolytes as flocculants to aggregate bacterial suspensions.

Chitosan (Figure 2) is an inexpensive, biodegradable, non-toxic, cationic natural polymer/ polysaccharide obtained by *partial* (~50%) deacetylation of chitin found in the exoskeleton of crustaceans like shrimp (QIN et al. 2006). The cationic nature of chitosan is particularly desirable to flocculate and aggregate negatively charged particles. Bacterial cells contain large quantities of side chain amino acids, methyl groups attached to polysaccharides and long chain carbon groups found in lipids; all contributing to the hydrophobic and predominately negatively charged properties of cell membranes (Mozes, N, Amory, D.E., Leonard, A.J., Rouxhet 1989). In gram negative bacterial cells, the anionic phosphate and carboxyl group residing on lipopolysaccharides (LPS) of the outer membrane (OM) will electrostatically interact with the divalent cationic molecules of chitosan (Kong et al. 2010). Chitosan polyelectrolytes rely on electrostatic surface charges to engage in extra cellular polymer/particle interactions and therefore can bind to the negatively charged extracellular structures (Rinaudo 2006).

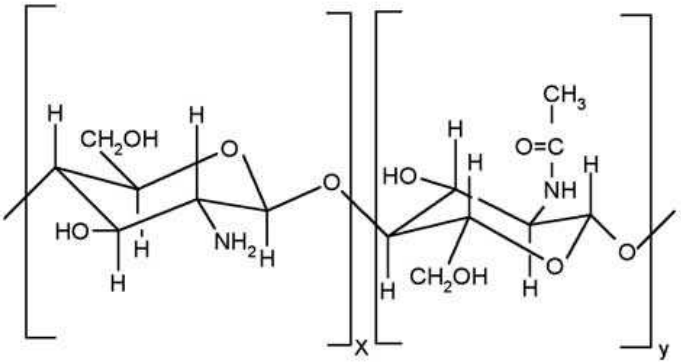

Figure 2. Structure of partially de-acetylated chitosan *(Rinaudo 2006)*.

Chitosan is soluble in slightly acidic conditions (Sugimoto et al. 1998; QIN et al. 2006) and can be categorized as any linear polysaccharide that has various proportions of (1→4) linked 2-acetamido-2-deoxy-β-D-glucopyranose (GlcNAc) and 2-amino-2-deoxy--β-D-glucopyranose

(Strand et al. 2001). The solubility of chitosan is complicated, challenging to control and largely effects the efficiency of flocculation and other applications The solubility of chitosan depends on the pH, degree of acetylation (DA) and molecular weight (MW). As a weak base chitosan is insoluble in pure water but soluble in slightly acidic solutions with pH < 6.5. To broaden chitosan's flexibility in application, much effort has been applied to performing chemical procedures like the Maillard reaction (Chung et al. 2011) to prepare functional, water soluble derivatives which has resulted in commercially available chitosan oligosaccharides of agricultural and pharmaceutical grade .

5.5.2 Shear Stress on Cells During Flotation

Production of biological products like therapeutic proteins, vaccines, and antibodies are commonly derived from cell products cultivated in industrial-scale bioreactors (Chisti 2000). Cell cultures require sufficient oxygen to remain healthy, so artificial aeration is particularly important for cell suspensions larger than 10,000 L (Ma et al. 2004) with high cell densities ($\geq 10^6$ CFU/mL). Gas sparging is a common method delivering oxygen to bioreactors. Although highly effective, this process induces lethal levels of hydrodynamic force to the cell resulting in bubble associated damage leading to cell lysis and death. Two mechanisms of cell damage can occur during sparged aeration. Firstly, hydrodynamic forces (*i.e.,* shear stress) at the gas-liquid interface as a bubble passes by and interacts with a cell, and secondly, cell death as bubbles rupture at the media surface (Walls et al. 2014). Additional cell damage can occur if the degree of turbulence of circulating media is especially intense resulting in high shear in the liquid phase itself (Chisti 2000; Sowana et al. 2001).

5.5.3 Pluronic F-68

Surfactants can change interactions between a bubble and surrounding biological material in a fluid by modifying the surface tension forces that typically attract, stress or disperse biomaterial ((Ma et al. 2004; Tharmalingam et al. 2008; Walls et al. 2014). Pluronic F-68 (Figure 3) is a commercially available non-ionic surfactant that has been widely investigated and shown to protect cells by masking hydrophobic surfaces on thereby reducing the effects of shear forces (Ma et al. 2004).

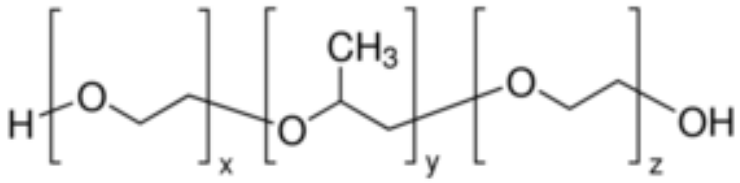

Figure 3. Structure of Pluronic ®- F68 (C3H6O.C2H4O)x

5.6 Pathogen Detection Model

5.6.1 Loop Mediated Isothermal Amplification (LAMP)

Isothermal nucleic acid amplification assays, like loop-mediated amplification (LAMP), are increasingly used on commercially available portable molecular diagnostic platforms. Although LAMP is often compared to polymerase chain reaction (PCR), a common nucleic acid amplification assay, there are notable differences that support LAMP as an ideal diagnostic tool for POC testing. Foremost, gene based assays like PCR require benchtop machinery to provide

sufficient power to support rapid thermal cycling between relatively large temperature extremes, *i.e.,* >90°C for heat denaturation of the double stranded DNA and ~50-60°C for primer annealing and extension. Unlike PCR, LAMP does not require heat denaturation of ds DNA and amplifies DNA under isothermal conditions *i.e.,* 65°C for 30 minutes. LAMP classically requires 4 separate primers: forward inner primer (FIP), forward outer primer (F3), backward inner primer (BIP), backward outer primer (B3) (Notomi et al. 2000). LAMP can be accelerated dramatically by the use of "loop" primers homologous to loops in the LAMP amplicon (Nagamine et al. 2002). After FIP anneals to the complimentary ds DNA target at 65°C (the condition of dynamic equilibrium for ds DNA) the intrinsic strand displacement of activity of the DNA polymerase initiates the complex LAMP amplification cascade through self-priming of loops in the amplicon, and additional priming with available inner primers.

LAMP is relatively insensitive to inhibitors commonly found in environmental and food sample matrices like polysaccharides, cellulose, humic acids and heavy metals (Wilson and Wilson 1997) enabling simple and field adaptable procedures (*i.e.,* crude cell lysis) to extract nucleic acid from a sample for downstream analysis (G. 2009). LAMP technology is rapid and can detect pathogens in 30 minutes or less while maintaining robust and sensitive detection of target DNA.

Diagenetix Inc., a startup company founded to commercialize diagnostic technologies developed at the University of Hawaii, manufactures a handheld portable molecular diagnostic device (BioRanger^{TM} , Figure 4) capable of detecting any gene marker of a virus or microbial pathogen by LAMP. LAMP technology is compelling for use in rudimentary labs and in the field however practical application of LAMP is bottlenecked by the dependence on sample preparation. For this research, I chose to directly evaluate the ability of electroflotation sample treatment to increase sensitivity using LAMP as a molecular diagnostic detection model.

Figure 4. BioRanger™ (Diagenetix, INC.). A handheld biology lab that uses LAMP to detect any gene marker

6. MATERIALS & METHODS

6.1 PCB Electrode Arrays

Another MS student initiated foundational work for this research and designed the first iteration of PCB electrode arrays. For this design, electrolysis reactions were supported on planar, inert gold-plated PCB electrode arrays designed using a PCB CAD software (EAGLE, Autodesk, Mill Valley, California, USA) (Figure 5) patterned on custom printed circuit board (PCB) fabricated by a commercial manufacturer (OSH Park, Lake Oswego, OR, USA). The electrodes are arranged in horizontal pattern of concentric rings alternating between anode and cathode and separated by a space of approximately 1mm. Solder mask material was used to cover all of the conductors on the surface except for a grid of plated vias perforating the board in circular patters around the perimeter of each conductive track. Conductive polymers were then printed into the vias to protect the underlying / exposed metal, and to provide electrical contact to the electrolyte. Electrodes were housed in a custom milled acrylic base that connects to the EF cartridge. A silicone gasket pressed between the cartridge and the base provided a seal to prevent leakage of the media. The housing assembly for the PCB electrodes was different than the final EF system housing design, primarily to enable connection to the different electrode arrays manufactured in the respective implementations. The design used for the PCB arrays is not shown here as we did not ultimately use them for extensive testing of the electroflotation process itself.

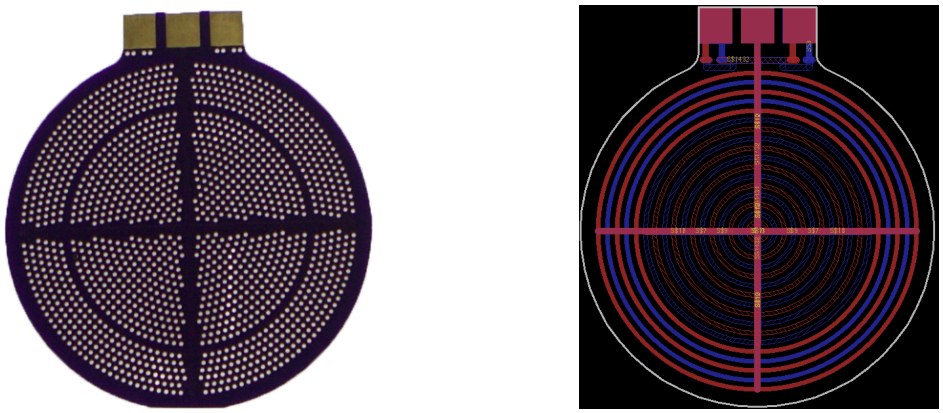

Figure 5. Image and electrical schematic of PCB electrode array. (left) PCB electrode array without corrosion coating. (right) EAGLE CAD schematic of electrical routes of inner anode (red cross-hatch), inner cathode (blue cross hatch) outer anode (solid red), outer cathode (solid blue).

6.2 Electrode Cleaning

To remove contaminants like ionic salts, oils or other particulates that could result in delamination of the conductive coatings, the PCB electrode arrays were cleaned using ultrasonic cavitation. The PCB arrays were placed in a beaker containing acetone inside the chamber of a CUBEX Sonic-3D for 5 min at 40 kHz at 25°C. After sonication, the electrodes were rinsed liberally with DI water, then dried and stored in sterile petri dishes.

6.3 Methods to Evaluate Corrosion Inhibiting Coatings

The following sections describe the materials and methods used to evaluate conductive pastes and adhesives as corrosion- resistant coatings for PCB electrode arrays:

1. Silver filled conductive epoxy
2. Carbon conductive paste
3. Graphite filled silicone

While extensive testing was done using PCB electrode arrays, the final electrode arrays selected for use in electroflotation experiments were commercially manufactured titanium platinum electrode arrays. Characterization of electrolysis on the titanium platinum (TiPt) electrodes is summarized at the end of this section.

6.3.1 Methods to Evaluate Ag Epoxy

A sample EP21TDCS Silver Filled Epoxy was obtained from Masterbond (Hackensack, NJ, USA) as a previously cured sample on a glass slide.

6.3.1.1 *Electrolytic Cell*

Electrolysis is a process by which thermodynamically favored redox reactions are reversed by the application of an external electrical potential/ energy. The relative thermodynamics and kinetics of different redox reactions with respect to the applied potential will determine which of the components in the electrolyte or electrodes are oxidized or reduced, and the rates at which these reactions occur. As a rule of thumb, electrolysis will occur first for paired half reactions with the nearest reduction potentials, though if one or both of these reactions require significant activation energy an overpotential will be required to support the desired reaction rates. However, application of overpotentials can result in undesirable redox reactions such as corrosion of electrodes or formation of reactive chlorine species.

A simple electrolysis cell was constructed to examine the cyclic oxidation and reduction of silver epoxy. A silver poxy electrode and stainless-steel counter electrode were submerged in 250 mL of a saturated KCl solution (4.56 M). A programmable DC power supply (Model E3632A, Agilent Technologies, Santa Clara, CA, USA) was used to apply desired potential, and handheld multimeter (Model 115/EFSP, Fluke Corporation, Everett, WA, USA) was used to measure the

resulting current as shown for corresponding oxidation (Figure 6) or reduction (Figure 7) processes. Initially an oxidative potential of 0.888 V was applied to the silver epoxy electrode relative to the steel electrode, and current monitored for 180 minutes. We then tried to recover the reduced elemental silver by applying a reduction potential (-1.5V) for 180 minutes, followed again by the 0.888 V oxidation potential for 180 minutes.

In the constructed cell:

$$E°_{cell} = E°_{oxidation} + E°_{reduction}$$

$E°_{reduction}$: $2H^{1+}_{(aq)} + 2e^- \rightarrow H_{2\,(g)}$ $E°= 0.00$ V **Eq. 7**

$E°_{oxidation}$: $AgCl + e^- \rightarrow Ag + Cl^-$ $E°= 0.22$ V **Eq. 8**

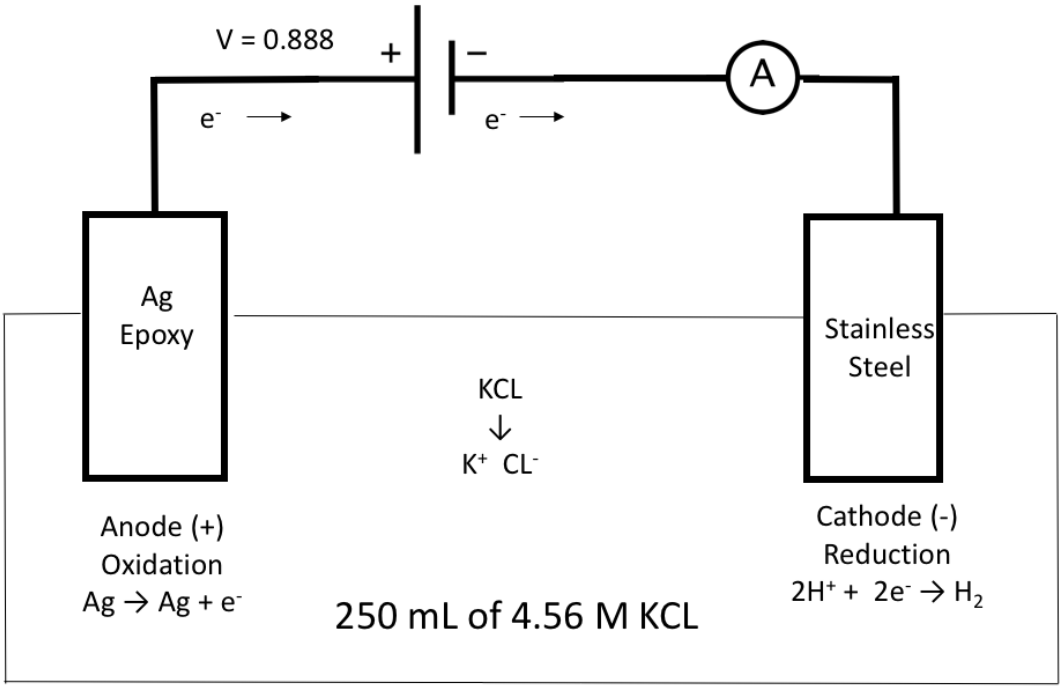

Figure 6. Electrolytic cell setup for oxidation of Ag epoxy

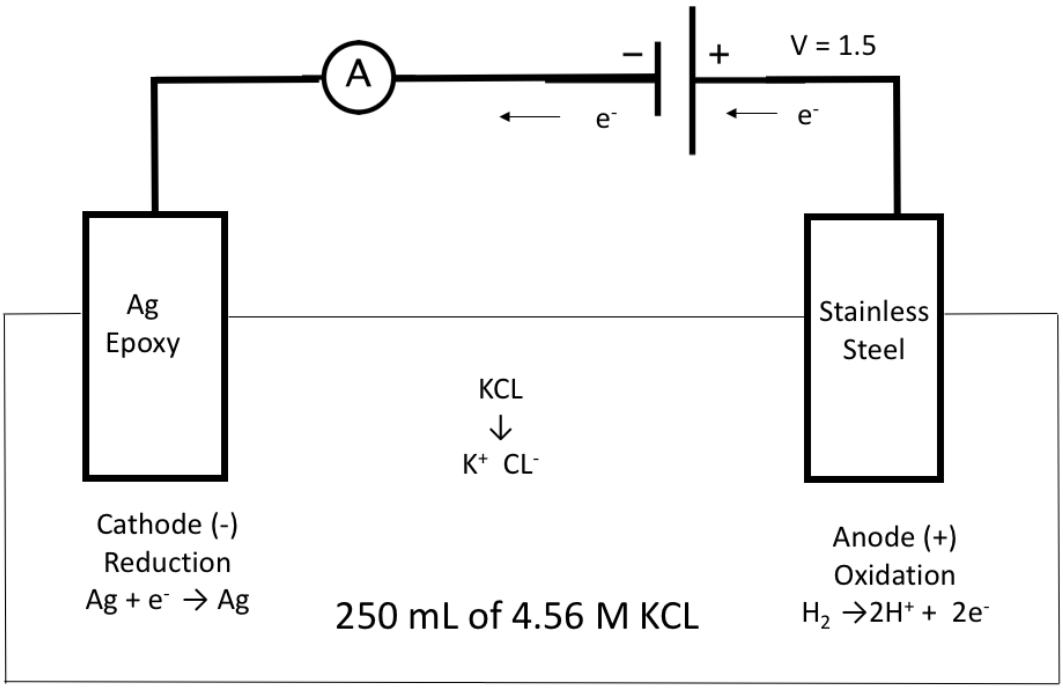

Figure 7. Electrolytic cell setup for and reduction of Ag epoxy

6.3.1.2 Scanning Electron Microscopy & Energy Dispersive X-ray Spectroscopy

Corrosion morphologies were imaged using scanning electron microscopy (SEM), (Hitachi S-4800 Field Emission model) followed by energy dispersive X-ray spectroscopy (EDS) (Oxford INCA X-Act EDS system) to measure the changes in compositional characteristics of the Ag epoxy electrodes after each 180-minute period of oxidation and reduction. SEM and EDS imaging were conducted at the Biological Electron Microscopy Facility in conjunction with the Pacific Biosciences Research Center at the University of Hawaii at Manoa. SEM allows for high resolution imaging of surface structures with a nanometer range resolution. EDS is a semi-quantitative analysis in which the energy of backscattered electrons images resulting from elastic collisions

with atomic nuclei of different atomic numbers can be used to infer presence and composition of different elements on the material surface. The analysis is confined to a user set SEM window area and results show what elements are present in the material and relative percent (%) compositions (Hafner, B. 2006). EDS is a valuable technique to evaluate effects of corrosion, providing analysis of chemical composition of metal oxides during passivation of the metal (Zarras, P, 2003., Lim et al., 1998). SEM visualizes morphology and chemical composition of a material, and in this application, can show changes over time under different conditions and material degradation in a corrosive environment (Wessling, B, 1999).

6.3.2 Methods to Evaluate Carbon Conductive Paste (CCP)

CCP 7102 was purchased from DuPont. It is a conductor with low sheet resistivity (20-30 ohms/sq/mil), high stability and rated to exhibit excellent adhesion to many types of substrates. 7102 is a black paste with high viscosity (60-125 Pa.S) and composed of dipropylene glycol methyl ether (60-70%), carbon black (10-20%), graphite (10-20%), polyether resins (10-20%) and small percent fatty acid salts of polyamine (0.1%-1%). CCP's generally have a hydrophobic surface characteristic due to the presence of lipophilic binders. Furthermore, the higher the lipophilic percent composition in the CCP, the slower the rate of charge transfer within the material and on the surface. Therefore, by reducing the amount of liquid in the CCP or subjecting the CCP to electrolysis which induces surfaces hydrophilization, the more rapid the charge transfer (S˘vancara,, I. , 1996). Based on the composition of CCP 7102 as described in the MSDS, appropriate volumes of graphite power (G67-500, Grade 38, Fisher Chemicals) were added to 7102 and vigorously mechanically mixed to achieve a final composition of 50% graphite. CCP 7102 was screen-printed to fill and cover the exposed vias in the cleaned PCB electrode array using

an AMI/PRESCO manual screen printer with a vacuum chuck. The stainless-steel screen/stencil was designed using a CAD software (EAGLE, Autodesk, Mill Valley, California, USA) and commercially fabricated (PCB Unlimited, Inc., Tualatin, OR, USA). After application, the PCB + CCP was cured in a box oven for 10 min at 120°C. The CPP application process was repeated twice curing the material each time.

The patterned and cured CCP + PCB electrodes were placed in a test EF system containing 400 mL of 0.1 M potassium phosphate electrolyte for 40 minutes with an applied potential of 4.21 V. Voltage, time and current (mA) data was logged using the microcontroller and custom developed AndroidOS application described in section 6.5 "Control System".

6.3.3 Methods to Evaluate Conductive Silicone

A two component, graphite filled electrically conductive Silicone, Mastersil 155 was purchased from Master Bond (Master Bond Inc., Hackensack, NJ, USA). Mastersil 155 is a silicone based rubber with repeating units of poly-dimethyl-siloxane (PDMS). When cured, Mastersil 155 is rated to have a volume resistivity of 20-40 ohm cm^{-1} and a conductivity of 20-30 ohm cm^{-1} at 75°C. Mastersil 155 was patterned onto PCB electrode arrays using the same screen printing method and stencil as described in the CCP methods section. After application, the PCB + conductive silicone was cured in a box oven for 30 min at 225°C.

Plasma treatments were conducted using a table top Harrick Plasma Basic Cleaner PDC-32G. Constant chamber pressure (250 mTorr), oxygen flow rate (1-1.5 kg/cm^2), and RF power (18 W) were all kept constant for plasma oxidation for a total plasma exposure time of 5 min. Immediately following plasma treatments Functional OH^- groups were grafted onto the surface of conductive silicone by submerging the electrode array in PEG in a glass petri dish for 5 min. After

grafting PEG, the electrode array was rinsed liberally with DI water and used in varying conditions of EF treatments. Images were taken of electrodes during electrolysis before and after plasma and grafting treatments. The patterned and cured conductive silicone + PCB electrodes were placed in a test EF system containing 400 mL of 0.1 M potassium phosphate electrolyte for 3-10 minutes with varying constant applied potentials (3-6 V). Voltage, time and current (mA) data was logged using the microcontroller and custom developed AndroidOS application described section 6.5 "Control System".

6.4 Platinum Coated Titanium Electrode Arrays

Electrolysis reactions are supported on inert platinum (Pt) plated grade 1 titanium (Ti) electrodes (Figure 8, left**)** custom designed using a 3D CAD design software (SOLIDWORKS 2016, Waltham, MA) (Figure 8, right) and fabricated by a commercial manufacturer (Baoji Qixin Titanium Co. Ltd, Maying Town, Weibin District, Baoji, Shaanxi, China). Carefully considering the spatial arrangement of electrodes is important to maintain high electrolysis efficiency (Nagai et al. 2003). To minimize ohmic losses and application of potentially corrosive over-potentials, electrodes are arranged in a horizontal pattern of concentric rings alternating between anode and

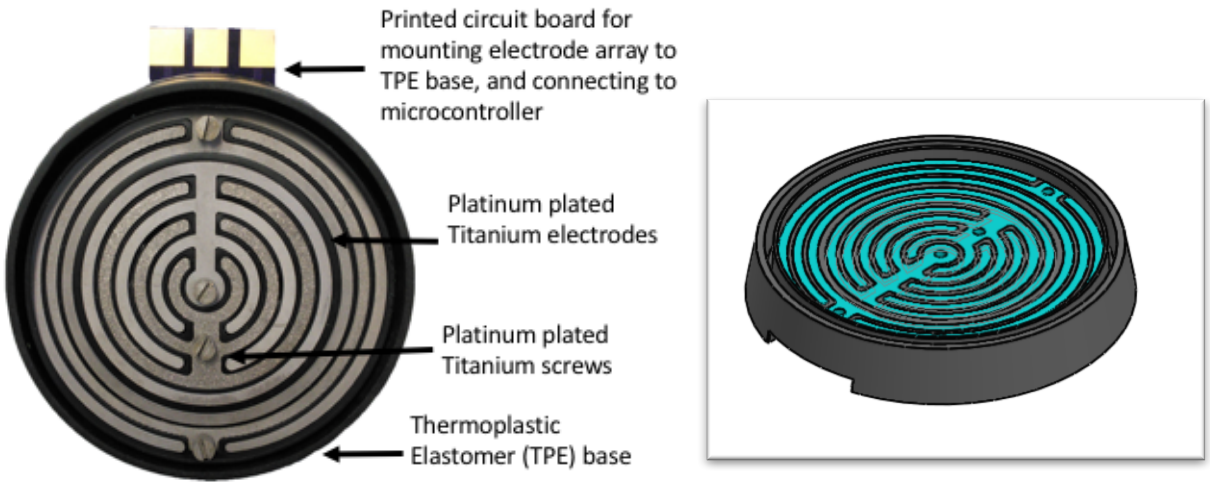

Figure 8. Platinum coated Titanium electrode array assembly (left). Top view. Solid Works drawing of TiPt electrode arrays (turquoise) with silicone base (grey)(right). The outer diameter of the base is 76.5 mm.

cathode and separated by a spacing of 1 mm (Alam and Shang 2016). The thickness of the electrodes was chosen to be 2 mm. The system consists of two individual sets of electrode arrays, each designed to generate bubbles in defined areas of the EF cell (see section "electroflotation cell and process"). The inner anode has a surface area (SA) of 826.05 mm^2 with corresponding cathode SA of 622.57 mm^2 while the outer anode has total SA of 880.02 mm^2 with corresponding cathode SA of 436.32 mm^2. Surface areas are calculated considering only the area of the exposed electrode face. Electrode arrays are housed in a custom engineered thermoplastic elastomer base (TPE) (3D Systems Inc., Atlanta, GA, USA) (Figure 2) that electrically isolates adjacent electrodes from one another and provides a seal preventing leakage of electrolyte out of the EF cartridge and onto the attached electrical control system.

6.4.1 Methods to Evaluate Platinum Coated Titanium Electrodes

TiPt electrodes were tested at 20 minutes at high and low constant applied current in the EF cell (described in section 6.6) using a control feature to maintain a desired constant current (see

section 6.5 “Control System”). These electrodes were used in all subsequent electroflotation experiments described in later sections. I evaluated the stability and corrosion resistance by observing how much the required potentials changed to support the designated current values over time i.e. high and low current settings. EF treatments performed at high turbulence flotation settings (see section 6.9) were used to evaluate high current settings i.e. 600 mA. EF treatments performed at low turbulence flotation settings (see section 6.9) were used to evaluate low current settings i.e. 300 mA. Voltage, time and current was recorded and logged using the EF system microcontroller and AndroidOS application. The logged current (mA) data from 3 experimental replicates at high and low current was averaged and reported.

6.5 Control System

Current through the electrode arrays is controlled with a custom circuit assembly connected to the electrodes with platinum plated titanium screws (Figure 8). The circuit is controlled with an 8-bit microcontroller (Atmega-328P, ATMEL Inc., San Jose, CA) interfaced through a Bluetooth modem (RN42, Microchip Technology, Chandler, AZ) to a custom Android application (Figure 9) that allows user control of process parameters including process durations (min.), voltage (3.5-12 V), current (0-1000 mA), frequency (0-100 Hz), and duty cycle (1-100%). The current control feature allows a desired current (I) to be maintained throughout the EF process irrespective of the media composition/electrical characteristics, and subject to the constraints of the available voltage range. Feedback control of voltage (or current) on two sets of concentric electrode arrays is achieved by measuring cell currents and voltage with two bi-directional current/power monitors (INA219, Texas Instruments Incorporated, Sunnyvale, CA 94043), and adjusting the voltage output through a switching regulator (LT1373, Linear Technology Corporation, Milpitas, CA

93035) network controlled with a digital potentiometer. In general, the greater the applied voltage or current, the more vigorous the electroflotation process will be. An outline of communication and information transmission is demonstrated in a block diagram (Figure 10). Current and voltages were recorded at the end of each pulse applied to the electrodes.

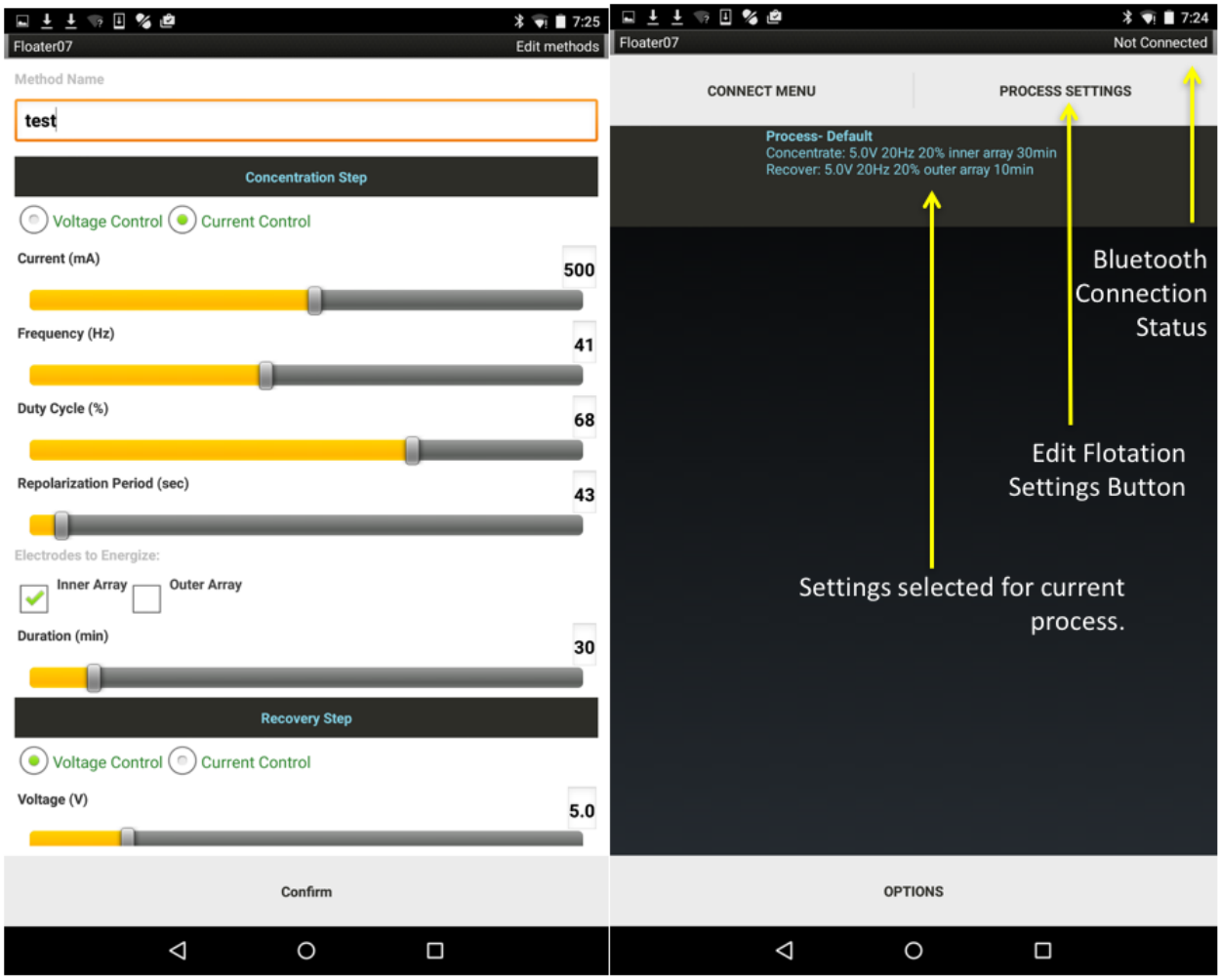

Figure 9. AndroidOS application user interface Home Screen (right) and Process Settings Window (left)

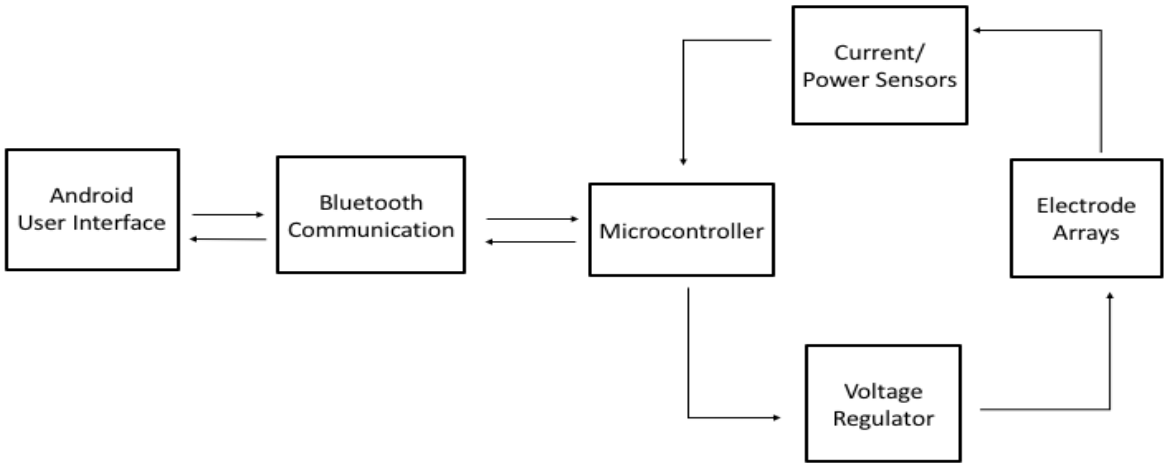

Figure 10. Block diagram of control system information pathway.

6.6 Electroflotation Cell for Automated Concentration and Recovery

The cylindrical electroflotation cell (Figure 11) housing is made of custom machined cast acrylic tubing and rod where generated gas is partitioned into one of two headspaces: a collection chamber in the core of the cylinder that vents to the atmosphere, and a concentrically arranged trap where gas can accumulate to displace media from the collection chamber. After the sample is loaded into the flotation chamber (Figure 12A), the electroflotation treatment consists of two main process events: (1) concentration step (Figure 12B) and (2) recovery step (Figure 12C). During the concentration step the inner set of electrode arrays are energized (Figure 12D), allowing collimated microbubbles to flow upward directing particulates into the collection chamber. After a user defined duration (min.), the recovery step is initiated, and both the inner and the outer set of electrode arrays are energized such that gas also begins to accumulate in the trap. As gas accumulates in the trap, material concentrated in the collection chamber is displaced through a dispensing tube where it is collected by the user into defined volume fractions (mL).

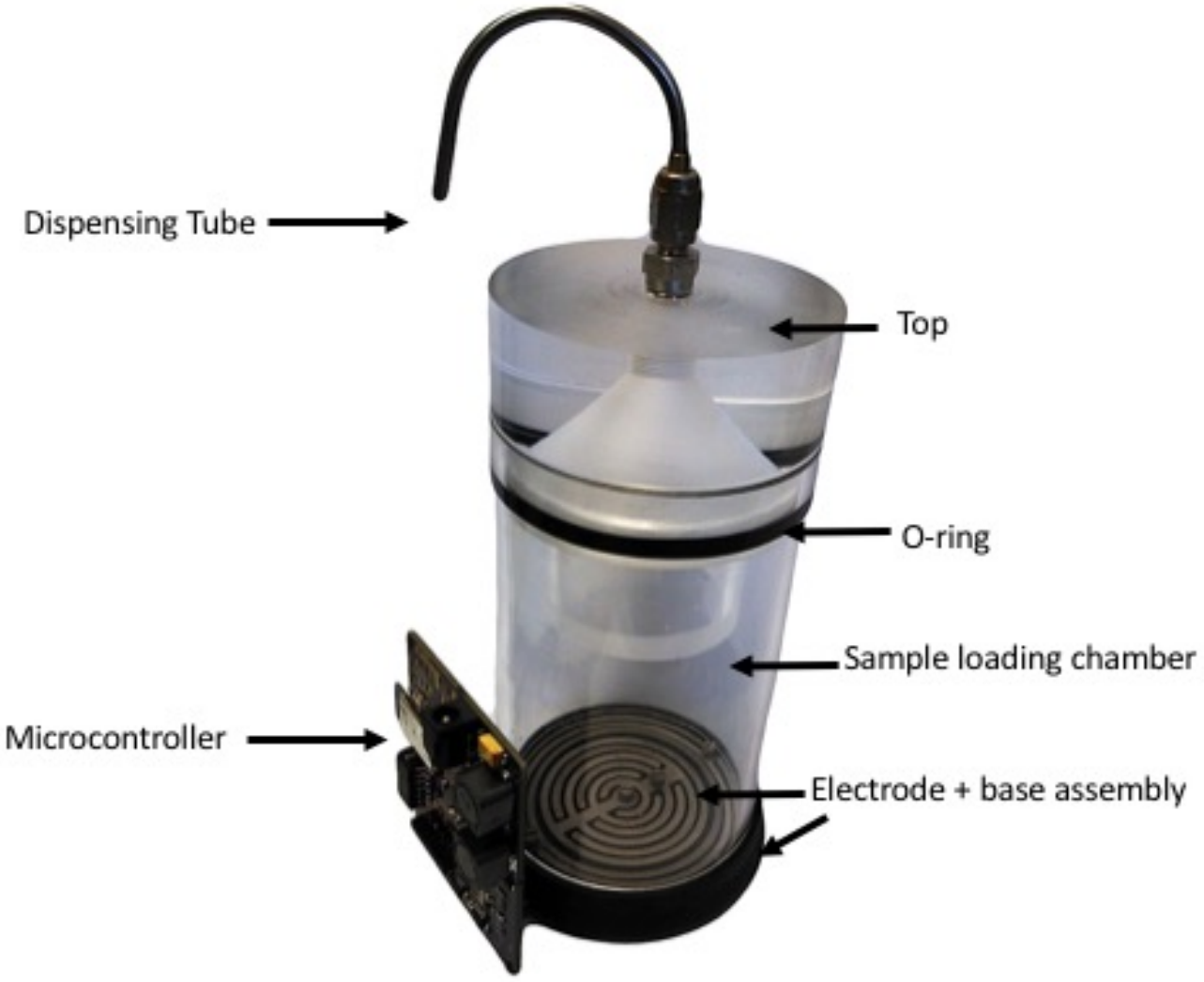

Figure 11. Image of assembled electroflotation cartridge.

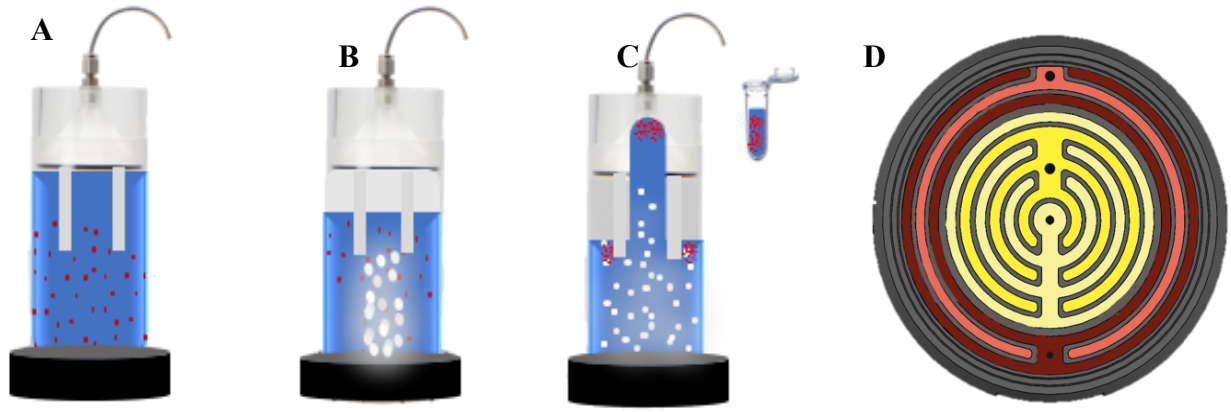

Figure 12.(A-C) Sequence (left to right) of electroflotation process for concentrating and recovering suspended particles (red dots). The sample is loaded into the chamber (A), inner electrode arrays are energized to concentrate particles in collection chamber(B), and inner and outer electrodes arrays are energized to displace concentrated sample (C). (D) Electrode array schematic. Inner array is shown in yellow, and outer array is shown in red. The grey area corresponds to the TPE housing

6.7 Preparation of Bacterial Cultures and Media

As a model organism to test the efficacy of EF treatment, a non-pathogenic isolate of *E. coli* (ATCC strain 25922) was grown overnight on plate-count agar (Difco™) at 37°C. Colonies were then transferred into sterilized potassium phosphate buffer (0.1 M, pH 6.6) adjusted to achieve an absorbance of 0.13 at 600 nm as read on a commercially available spectrophotometer (Healthcare Ultraspec™ 10, General Electric, location). This absorbance was shown empirically to be equivalent to about 10^8 CFU/ml ($\bar{x}$ =1.63 x 10^8 CFU/mL, s =2.55x10^2 CFU/mL, n=3) through comparison to standard plate counting methods. Bacterial cultures and media were freshly prepared for each electro-flotation experiment.

6.8 Preparation of Electroflotation Bacterial Suspension Samples

Phosphate buffer (0.1 M, pH 6.6) was used as the media to facilitate electrolytic charge transfer and moderate pH changes from half reactions at the electrodes. We inferred a conductivity (κ) for this media of 12.8 mS/cm from acid dissociation and ionic conductivity data reported in the literature (Lide 1994). Electrically conductive media is important to support high electrolysis rates efficiently with minimal over potential, and minimize corrosion and other undesirable redox reactions (Nagai et al. 2003; Chen 2004). The pH was measured using an AB15 Plus meter (Accumet Basic, Fisher Scientific) and buffer was sterilized in an autoclave before inoculation. 380 mL of sterile phosphate buffer was inoculated with appropriate volumes of freshly prepared *E. coli* 25922 culture in 500 mL sterilized flasks to achieve the following bacterial suspension concentrations: 10^2, 10^3, 10^4, 10^5 or 10^6 CFU/mL (Figure 8B). To homogenously disperse bacteria in suspension, samples were mechanically shaken briefly (90 seconds) after inoculation and used promptly for subsequent electro-flotation experiments. Control samples were prepared identically to EF samples, except instead of recovery via media displacement, fractions were collected with pipettes directly from the freshly prepared media.

6.9 Electroflotation of *E. coli 25922*

Prepared electro-flotation samples were gently poured into the electro-flotation chamber and sealed. To investigate the effects of varying EF treatment durations, samples were subjected to 10, 15, and 20 minutes of EF treatment. The "stirring effect" caused by rising clouds of bubbles (Zimmerman et al. 2008) can cause fluid to circulate, which may positively impact the collection efficiency by increasing particle/ bubble collisions (Kyzas and Matis 2014; Walls et al. 2014; Alam and Shang 2016) and rate of mass transport (Szpyrkowicz 2005) by bubbles (Szpyrkowicz 2005).

On the other hand, when bubble flux exceeds a critical limit, hydrodynamic forces due to turbulence in fluid circulation acting on suspended cells can break fragile flocs of cell aggregates causing shear stress or damage to cells (Elias et al. 1995; Sowana et al. 2001; Nagai et al. 2003; Sharma et al. 2005). Furthermore, excessive mixing due to the "stirring effect" could prevent cells from concentrating at the surface of media in the column, decreasing recovery efficiency. In summary, low turbulence conditions are a gentle process producing bubbles in a "laminar" flow column (Figure 13), but may result in slower or less efficient capture of suspended particles, while high turbulence conditions generate a "stirring effect" (Figure 14) to increase cell-bubble collision, but may break apart aggregated cell flocs (Figure 7). The flux rate bubbles, defined by volumetric rate of bubbles passing through a cross sectional area at any given time point, is most directly related to current density at electrode surfaces (Figure 14) (Chisti 2000; Nagai et al. 2003; Chen 2004). We observed that bubble flux and average bubble diameter were also dependent on frequency and duty cycle applied to electrodes. Lower frequencies and duty cycles, at the same current levels, generally resulted in smaller bubbles and less mass flux, as individual bubbles stopped growing and were more likely to randomly detach from electrode surfaces during the longer "off" periods.

Based on empirical observations of amount of turbulent mixing, I selected a "high turbulence" (HT) test condition to 500mA/ 100 Hz/ 75% duty cycle for concentration and 650 mA/ 100 Hz/ 75% duty cycle for recovery. To achieve conditions with less turbulent mixing where bubble flux is highly collimated during concentration, I designated a "low-turbulence" (LT) test condition performed at 300mA/ 20 Hz/ 30% for concentration and 600mA/20 Hz/ 50% duty cycle for recovery. The reported currents were taken as the sum of the current through both inner and outer electrode arrays (where the current through the outer arrays was effectively 0 during the

concentration step), measured at the end of the energized part of the cycle. A larger total current was always applied during recovery step because the current was distributed across both sets of arrays. In summary, inoculated EF samples were subjected to EF treatments at 27°C varying duration (10, 15 and 20 minutes) for all bacterial concentrations (10^2-10^4 CFU/mL) at different levels of flotation turbulence (high, low) (Table I). Three experimental replicates were performed for each treatment. The summary and experimental outline are detailed in Table 1 and Figure 15 respectively.

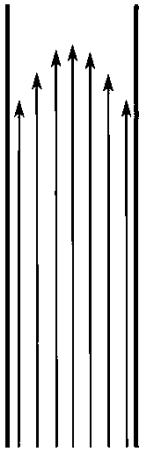

Figure 13. Behavior of bubble flux for low turbulence flotation conditions

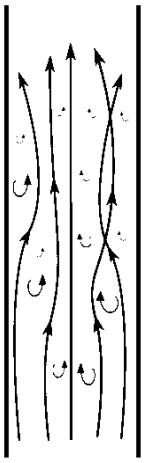

Figure 14. Behavior of bubble flux for high turbulence flotation conditions

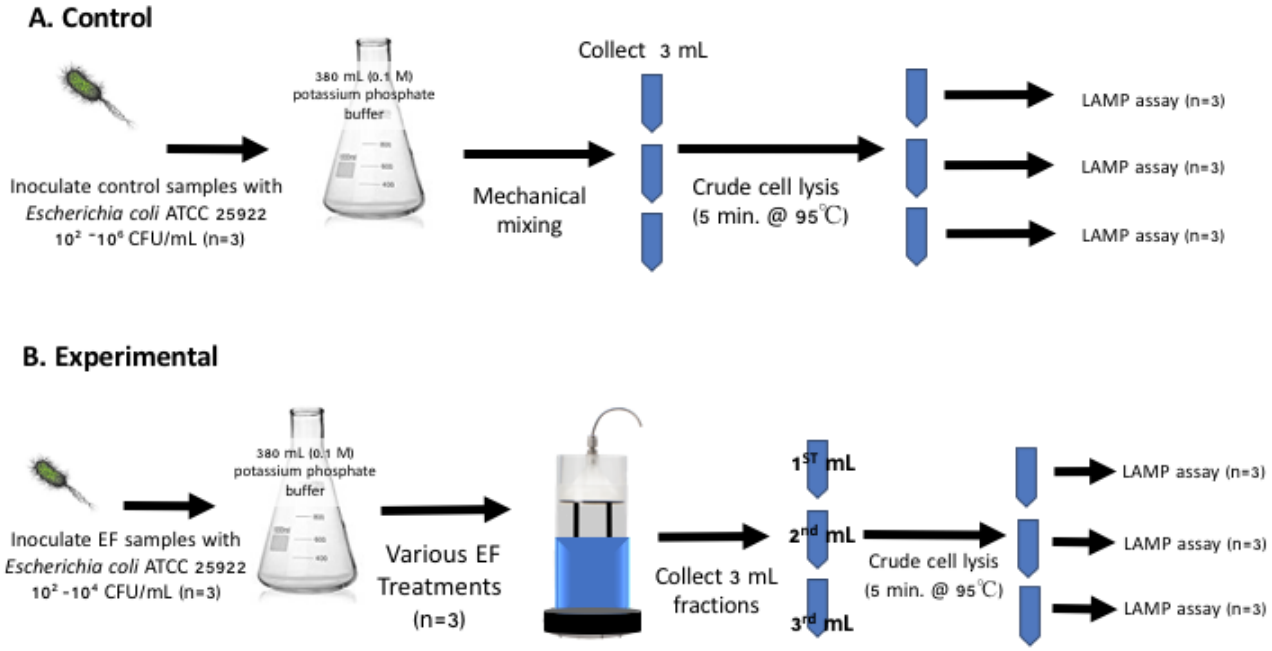

Figure 15. Electroflotation of E. coli experimental outline for control samples (A) and electroflotation samples (B).

Mixing Condition	CFU/ mL	EF Duration (Min.)	Mixing Condition	CFU/ mL	EF Duration (Min.)
Low Turbulence 300mA 20Hz 50% Duty Cycle	10^2	10	High Turbulence 500 mA 100 Hz 75% Duty Cycle	10^2	10
		15			15
		20			20
	10^3	10		10^3	10
		15			15
		20			20
	10^4	10		10^4	10
		15			15
		20			20

Table I. Experimental matrix of tested EF treatment conditions

6.10 Recovery of Electroflotation Treated Samples

To observe partitioning effects in electroflotated media, the first 3 mL displaced from every EF treatment condition were collected into individual 1 mL fractions in 1.5 mL Eppendorf tubes. DNA from all recovered fractions was extracted using crude cell lysate method (95°C for 5 minutes) (Teh et al. 2014), followed by 15 seconds of low speed vortexing. The recovered samples were later used in downstream molecular testing in a LAMP assay to evaluate the recovery of detectable cellular material by EF.

6.11 Development of a Loop Mediated Isothermal Amplification (LAMP) Assay

For detection of *E. coli,* we chose to use LAMP, a popular isothermal amplification chemistry that may be especially attractive for use in portable diagnostic systems (Kubota et al. 2011; Kubota and Jenkins 2015a). To target *E. coli 25922* we modified a previously published LAMP primer set (Teh et al. 2014) that we designated EcolC 3109_0 (Table II), targeting a conserved glycerate kinase coding region (EcolC 3109, Accession number: CP000946) of generic *E. coli* ATCC 8739. Evidently outer primers play a critical role in locally destabilizing inner primer annealing sites on template DNA to initiate the LAMP reaction cascade, so that proximity of outer primers to their corresponding inner primers can have a large effect on assay performance (Kubota et al 2011). Genome sequences returned from NCBI BLAST (https://blast.ncbi.nlm.nih.gov/Blast.cgi) for both ATCC 25922 and ATCC 8739 indicated that the forward outer primer (F3) target of EcolC 3109_0 was very distant from the FIP annealing site of EcolC 3109, suggesting a reason for poor performance we observed for this primer set in our own preliminary experiments.

We designed 5 alternative primer sets targeting the same single copy glycerate kinase gene from the *E. coli* ATCC 25922 genome sequence (NCBI GenBank, NZ_CP009072.1) including

forward loop primers (LF) as well as reverse loop primers (LB). The top five modified primer sequences were generated using PrimerExplorer V4 software (PrimerExplorer, Eiken Chemicals, Tokyo, Japan, http://primerexplorer.jp/e/), and after preliminary screening (data not shown) the most promising primer set, designated EcolC 3109_1 (Table III), was selected for further use in this study. Experiments to compare performance of primer set EcolC 3109_1 to the original primer set EcolC 3109_0 were conducted using serially diluted DNA purified using a Wizard genomic DNA purification protocol (Promega Corportation, Madison, WI), from *E. coli* ATCC 25922 DNA. Absorbance (260 nm) of purified DNA was measured with a NanoDrop 1000 DNA spectrophotometer (Thermo Scientific) to estimate DNA concentrations. The copy number of template genomic DNA was estimated by mass, assuming a genome size of approximately 5.2 Mbp WITH 50.4% GC content, resulting in a genome mass of about 17 fentograms. Purity was determined by taking the absorbance ratios at 280/260 nm and 250/230 nm. All LAMP assays were conducted in triplicate.

Table II. Original EcolC 3109_0 LAMP Primer sequences (Teh et al. 2014) for amplification of the glycerate kinase gene region of generic *Escherichia coli* 25922

Primer	Nucleotide Sequence (5' → 3')
Forward Outer (F3)	GGTAGATCGAACGGTCATCG
Backward Outer (B3)	GGCCAGCAACGGATTACG
Forward Inner (FIP)	CGCAGACTTCAAGCGTCACGATCGAAGGAACGGTGGATGC
Backward Inner (BIP)	CCTTACCGGCGACGGGAAAACTTTTCAGGCGCGACCAG
Reverse Loop (LB)	TGAGATGGCGGCAGCAAGTG

Table III. Modified Ecol 3109_1 LAMP Primer sequences for amplification of the glycerate kinase gene region of generic *Escherichia coli* 25922.

Primer	Nucleotide Sequence (5' → 3')
Forward Outer (F3)	GGCGAATGCCGTTATCCAG
Backward Outer (B3)	CGTGACGCTTGAAGTCTGC
Forward Inner (FIP)	CGCGCCTGAAAAGCGTAATCC CGCATGACGAATCAGCTCTC
Backward Inner (BIP)	CAATCACCGCCGTTTTCCCGT CGATGGGCGAAACAGTGAAT
Forward Loop (LF)	TGCTGGCGTCAAGTTTTGG
Reverse Loop (LB)	CGCCGGTAAGGCCATAAAAA

6.11.1 LAMP Primer Reaction Conditions

All LAMP reactions using the modified primer set EcolC 3109_1 and original primer set EcolC 3109_0, were performed in 25 μL (total volume) containing 40 pmol of each inner primer (BIP and FIP), 5 pmol of each outer primer (B3 and F3), 20 pmol of each loop primer (LB and LF where applicable). Reactions were prepared by adding 5 μL of a stock primer solution and 5 μL of sample to 15 μL of commercially available Isothermal Mastermix with dye (Catalog No. ISO001, Optigene, Inc., Horsham, UK). All primers were synthesized commercially (Integrated DNA Technologies, Coralville, IA, USA). All reactions were performed in 0.1 mL TempPlate semi-skirt PCR 96-well Plates (Catalog No. 1402-9100, USA Scientific, Inc., Ocala, FL, USA) in a commercial real-time PCR machine (Applied Biosciences StepOnePlus^{TM}) incubated at 65°C for 31 minutes. Fluorescence values were recorded every 30 seconds during the 31 minute reactions. The "threshold time" t_T was estimated as the amount of time required for the fluorescence value to exceed a threshold value equivalent to the pooled average plus three standard deviations of the

fluorescence values observed throughout reactions of triplicate negative control reactions (Kubota and Jenkins 2015a; Kubota and Jenkins 2015b). Reported averages of t_T values exclude assays with undefined t_T values (t_T >31 minutes). Reactions were conducted in triplicate for each template DNA concentration and primer set, including for the non-template controls.

6.11.2 LAMP Primer Sequence Identity Among Generic *E. coli* Strains

To evaluate how conserved the primer annealing sites are among generic *E. coli* strains, *in silico* analysis was conducted on 58 published sequences of generic *E. coli* strains retrieved from NCBI GenBank database. The 58 sequences, including ATCC 25922, were aligned using BLASTn (https://blast.ncbi.nlm.nih.gov/Blast.cgi) against the modified primer set EcolC 3109_1. The BLASTn results were subsequently confirmed by multiple alignments of the sequences by using ClustalW v.2.1(Conway institute UCD Dublin, Ireland, ftp://ftp.ebi.ac.uk/pub/software/clustalw2/) and BioEdit v7.2.6.1 sequence alignment editor software (North California State University, USA) and a percent match (%) value was calculated considering only the primer annealing site and not the entire target gene region. To verify the specificity of the modified primer set 3109_1 to *E. coli,* 26 previously published complete genomes (Lu et al. 2014) of non-*E.coli* strains were tested *in silico* using BLASTn. BLASTn results generated a percent query cover using BLAST's local alignment algorithm to scan the entire imputed (query) genome for sequence similarities between non-*E. coli* strains and primer set 3109_1 that could cause non-specific primer annealing.

6.12 Evaluation of LAMP Assay Using Electroflotation Treated Samples

For detection of *E. coli* 25922 in recovered fractions from electro-flotation treated samples, 5 μL of crude lysed sample from each fraction (1^{st}, 2^{nd}, 3^{rd} mL) was directly used in an individual reaction tube (0.1 μL) under the previously described reaction conditions. Electroflotation experiments for each condition were conducted in triplicate. For every 1 mL fraction in each experimental replicate, 3 LAMP assays were performed. In parallel, a LAMP assay reaction curve was generated for control samples containing bacterial concentration of 10^2-10^6 CFU/mL without electro-flotation treatment in order to compare differences in threshold times (t_T) of samples subjected to varying electro-flotation treatment conditions (duration, turbulence level and initial inoculum level). Mean detection rates were calculated based upon the percentage of positive samples in 27 samples (9 samples/ experiment) (Wang and Turechek 2016). Detection was classified somewhat conservatively as a reaction with an observed threshold time (t_T) less than 28 minutes to reject false amplifications due to primer self-annealing and other effects, even though false amplicons could readily be discriminated by melting temperature analysis (unpublished data).

6.12.1 LAMP Detection Distribution Between Collected Fractions

In all experiments, the EF treatments were designed to concentrate bacteria dispersed in 380 mL into 3 fractions (1 mL each). Evaluation of the detection rates in the different fractions could help determine the level of stratification of cellular component near the surface, and the possibility that cells can be confined in a thin layer at the media surface. To better interpret the efficiency of concentration, each 1 mL fraction (1^{st}, 2^{nd}, 3^{rd}) collected from all experiments was analyzed individually for percentages of positive sample detection. Mean detection rates from each

fraction were calculated based on the percentage of samples with observed t_T < 28 minutes in 3 LAMP assays (3 assays/ 1 mL fraction), for each of the three experimental replicates at the given EF conditions.

6.12.2 Effect of Pluronic and Chitosan on LAMP

To test inhibitory effects on LAMP, varying concentrations of pluronic (0%, 0.05%, 0.1%, 0.5%, 1.0%, 2.0 %) and chitosan (0, $5x10^{-8}$, $5x10^{-7}$, $5x10^{-6}$, $5x10^{-5}$, $5x10^{-4}$, $5x10^{-3}$ g L^{-1}) prepared in sterilized DI water and 0.1 M phosphate buffer (pH 6.0) respectively were added to individual LAMP assays. 25 μL reactions were prepared by adding 5 μL of a stock primer solution (Ecol 3109_1) and 5 μL of sample containing 4 μL of tested concentrations of pluronic or chitosan and 1 μL containing 0.2 ng of purified (Wizard genomic DNA purification protocol, Promega Corporation, Madison, WI) *E. coli 25922* DNA to 15 μL of commercially available Isothermal Mastermix with dye (Catalog No. ISO001, Optigene, Inc., Horsham, UK). All conditions were tested in triplicate including positive and negative controls.

6.13 EF Treatments +/- Pluronic F-68

To enhance viable cell recovery, variable concentrations (0.001, 0.01, 0.1, 1 g L^{-1}) of pluronic (Pluronic ®F-68, non-ionic surfactant, Thermo Fisher Scientific Inc., Waltham, MA, USA) was added to the prepared EF bacterial cultures (10^2, 10^3 CFU/mL) and subjected to 15 min HT EF and 20 min LT EF. The 1st 3mL displaced from every EF treatment condition were collected into individual 1 mL Eppendorf tubes. DNA from all recovered fractions was extracted using crude cell lysate method (100°C for 5 min.) followed by 15 seconds of low speed vortexing. To increase DNA the quantity of DNA extraction, higher temperature (100°C) was used for crude cell lysis whereas 95°C was used in the foundational experiments section 6.10. For detection of *E. coli 25922* in recovered fractions from EF treated samples, 5 µL of crude lysed sample was directly used in an individual LAMP assay following identical LAMP primer reaction conditions and primer set EcolC 3109_1 also detailed in Objective 1. For every 1 mL fraction, 3 LAMP assays were performed. Three experimental replicates were performed for each treatment condition.

6.14 EF treatment +/- (Chitosan + Pluronic)

To aggregate cells producing shear protected flocs, variable concentrations of agricultural grade chitosan oligosaccharide (Figure 16) (soluble in pH 5-7) (Qingdao BZ Oligo Biotech Co.,Ltd, Qingdoa, China) (0.001, 0.01, 0.1, 1 g L^{-1}) was added to the prepared EF bacterial cultures (10^2 CFU/mL). Next, the cultures were placed on a shaker for 30 minutes at 50 rpm and then gently transferred to the EF cartridge and subjected to 20 min LT of EF treatment. Appropriate chitosan concentrations were prepared by serially diluting a stock concentration of 10 g L^{-} chitosan. The 1st 3mL displaced from the EF treatment condition was collected into individual 1 mL

Eppendorf tubes. DNA from all recovered fractions was extracted using crude cell lysate method (100°C for 5 min) followed by 15 seconds of low speed vortexing. To prevent LAMP inhibition, chitosan can be transformed from a DNA binding state to a DNA release state by adjusting the recovered fraction media pH (5.8) above the pKa (~9.5) of chitosan. To achieve this sample pH was adjusted from pH 5.8 to ~pH 10- 10.5 by adding 99 µL of 1 M NaOH to each 1 mL fraction incubated at room temperature for 10 minutes followed by 30 seconds of medium speed vortexing. For detection of *E. coli 25922* in recovered fractions from EF treated samples, 5 µL of crude lysed, adjusted pH 10 sample was directly used in an individual LAMP assay following identical LAMP primer reaction conditions using primer set EcolC 3109_1 as detailed in section 6.11.1 "LAMP Primer Reaction Conditions". For every 1 mL fraction, 3 LAMP assays were performed. Three experimental replicates were performed.

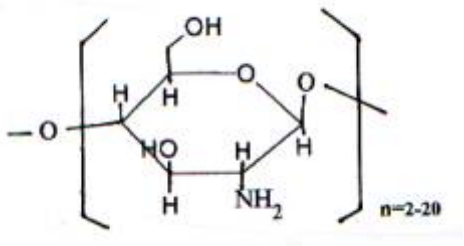

Figure 16. Structure of chitosan oligosaccharide (Qingdao BZ Oligo Biotech Co.,Ltd.) $(C_6H_{11}NO_4)n$ (n=2~20), pH 5-7. MW< 3000 Da)

6.15 Eluting DNA from Chitosan by Increasing Sample pH

To test if changing the pH of chitosan containing samples could release DNA from chitosan and prevent LAMP inhibition by chitosan, simulated EF samples were prepared containing 0.1 g L^{-1} pluronic and varying concentrations of chitosan (0.01 and 0.1 g L^{-1}). Appropriate volumes of dissolved chitosan stock (10 g L^{-} in sterile DI H_2O) was added to 0.1 M pH 6 phosphate buffer to

achieve a chitosan concentration of 0.01 and 0.1 g L^{-1} and distributed into 1 mL aliquots. Similarly, appropriate volumes of pluronic was added to achieve 0.1 g L^{-1} in all aliquots. Next, appropriate volumes of purified (Wizard genomic DNA purification protocol, Promega Corportation, Madison, WI) *E. coli 25922* DNA was added to each 1mL aliquots containing chitosan + pluronic + phosphate buffer and let to sit for 10 minutes. Next, the pH of some (Table IV: sample C, D) simulated EF sample aliquots was adjusted from pH 6 to pH 10 by adding appropriate volumes of NaOH and letting stand at room temperature for 10 minutes. pH was verified using an AB15 Plus meter (Accumet Basic, Fisher Scientific). Individual 25 μL LAMP assays were prepared by adding 5 uL of varying samples as described in Table IV to 15 μL Isothermal Mastermix and 5 μL of a stock primer solution (Ecol 3109_1). Three experimental replicates were performed for each sample type. Negative controls did not contain DNA or chitosan, while positive controls contained DNA in pH 10 phosphate buffer titrated with NaOH.

	LAMP Assay Sample Descriptions							
Sample Type	*E. coli 25922* DNA (ng)	DNA Volume (μL)	chitosan (g/L)	pH	DDnase Water (μL)	0.1 M Phosphate Buffer (μL)	1 M NaOH adjustment	Total Sample Volume (μL)
Negative	0	0	0		5	0	no	5
Positive	0.2	1	0	10	4	0	no	5
A	0.2	1	0.01	6	0	4	no	5
B	0.2	1	0.1	6	0	4	no	5
C	0.2	1	0.01	10	0	4	yes	5
D	0.2	1	0.1	10	0	4	yes	5

Table IV. Experimental design to test if increasing pH prevents LAMP inhibition by chitosan

6.16 Statistical Analysis

The performance of the electroflotation system is evaluated by effects on LAMP detection rates (0-100%) from samples subjected to various EF treatments in comparison to

control samples without EF treatment. Differences in detection rates based on positive detection in LAMP assays were evaluated using two-way ANOVA. Dunnett's multiple comparisons post-hoc analysis was used to identify experimental treatment conditions that were different than corresponding controls. Statistical differences in the detection rates from each fraction collected were evaluated using two-way ANOVA and post-hoc Tukey's multiple comparisons test. Detection rate data evaluating the initial EF system performance was normalized using a log transformation, however the data presented in figures is not transformed.

To evaluate the effects (i.e. inhibition) of adding pluronic and chitosan to a LAMP assay, differences in threshold times were evaluated by linear regression or two-way ANOVA and Dunnett's or Tukey's post-hoc analysis for multiple comparisons.

To quantify the effect of adding pluronic to EF treatments changes in LAMP detection rates from EF treatments + pluronic samples were compared to corresponding control samples from EF treatments without pluronic. The effect of chitosan was evaluated the same way except the control sample contained the 0.1 g L^{-1} pluronic.

"Reliable detection" was deemed to be positive identification of copies of template DNA or bacterial cells in at least 95% of assays at the tested condition. Positive detection was classified for threshold times values t_T<28 minutes. Averaged threshold times exclude t_T values (t_T >31 minutes). Significance was imputed for p-values less than 0.05.

7. RESULTS

7.1 **Corrosion Inhibiting Coatings**

7.1.1 Silver Filled Conductive Epoxy

7.1.1.1 Scanning Electron Microscopy

The silver epoxy, imaged by SEM prior to oxidation, shows an intact and smooth matrix (Figure 17, A). After oxidation (Figure 17, B), formation of holes and bubbles through the material was observed indicating the epoxy matrix had considerable changes in the physical morphology of the material.

A. B.

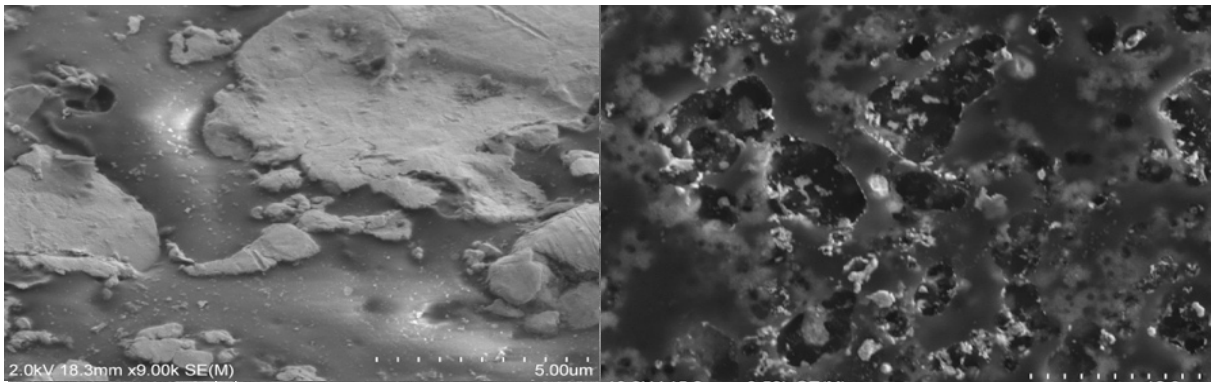

Figure 17. SEM images of silver epoxy. SEM image of untreated silver epoxy before oxidation (A). SEM image of silver epoxy after oxidation (B).

7.1.1.2 Energy Dispersive X-ray Spectroscopy (EDS)

The EDS results (Figure 18-20) confirmed that composition (%wt) of chlorine atoms on the untreated epoxy surface (Cl = 0.68%wt) changed after oxidation (Cl = 3.22 wt%) (Figure 18) and reduction (Cl = 2.0 %wt) (Figure 19). Percent weight (%wt) (Figure 20) is calculated as the relative concentration of the element at the surface of the sample i.e. silver epoxy in the viewing window of the SEM. At least some chloride present in the EDS analysis after reduction is likely

residual salt from the saturated KCl (4.56 M) solution (Figure 18, B). Although silver epoxy enabled hydrogen evolution at lower electrochemical potentials, and could be reversibly reduced, current (I) could not be sustained for long durations of time due to rapid chloridation and oxidation of the anodic surface. The rapid drop in surface conductivity of silver as it is oxidized to a coating of silver chloride paste renders silver epoxy as a poor choice for supporting intense anodic reactions for electrolysis.

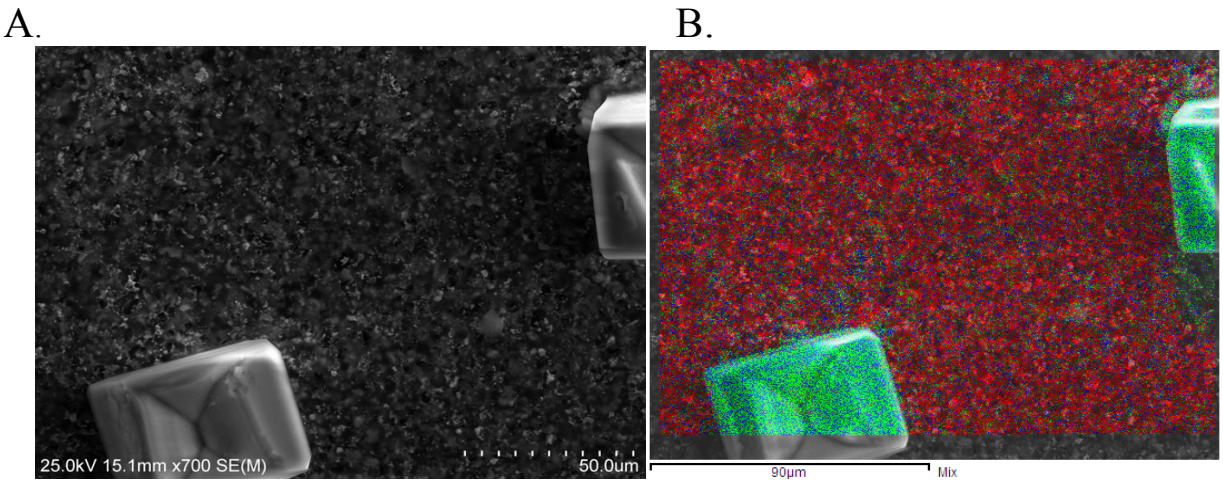

Figure 18. Overlaid EDS + SEM of silver epoxy after oxidation. (B) EDS distribution of Ag (red), K (green), Cl (blue) overlaid onto SEM image (A).

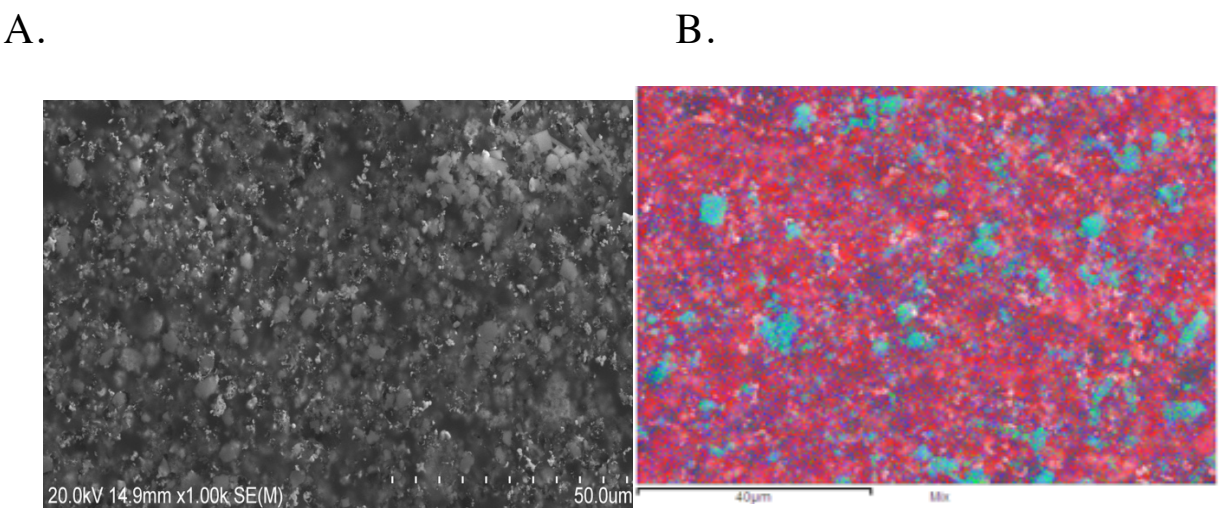

Figure 19. Overlaid EDS + SEM of silver epoxy after reduction. (B) EDS distribution of Ag (red), K (green), Cl (blue) overlaid onto SEM image (A).

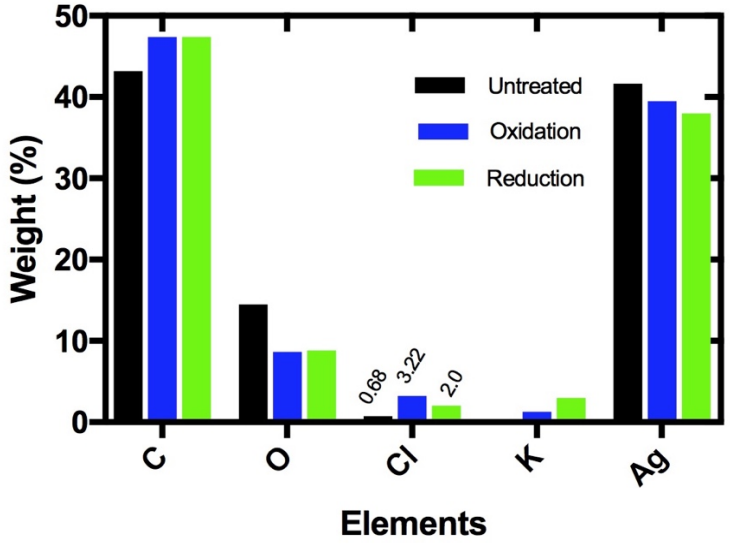

Figure 20. EDS percent weight (wt%) results of Silver Epoxy

7.1.2 Carbon Conductive Paste

PCB electrode arrays coated with CCP supported relatively stable current densities (1.5-14.2 mA/mm^2) at an applied constant voltage (4.21 V) over 120 minutes. Visible evidence of long term corrosion of the underlying metal was present on some, but not all, of the anodic surfaces of the electrode array (Figure 21, A). In (Figure 21, B), there is evidence that after ~75 minutes and 40 minutes for the inner and outer array respectively, the current sharply decreased. This suggests that for a short duration, e.g. for use in a disposable electrode array, CCP can adequately protect the underlying metal. However, without improved application and adhesion to underlying metal CCP may not be suitable for imparting long-term stability necessary for reusable electrode arrays.

A.

B.

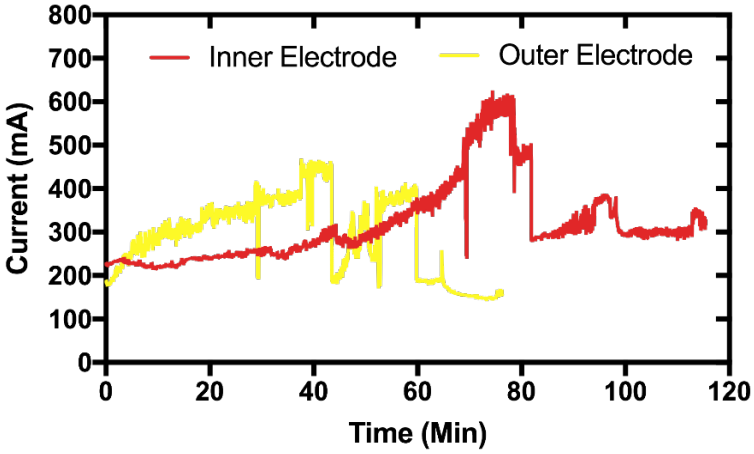

Figure 21. Image and recorded current (mA) of CCP coated electrode array subjected to EF. (A) Corrosion, (seen in blue) of PCB electrode array with applied CCP layer after 120 minutes of EF at 4.21 V in 0.1 M potassium phosphate buffer. (B) Current (mA) of inner and outer electrode arrays during 120 min. of EF treatment.

7.1.3 Conductive Silicone

Modifying the surface of PDMS by oxygen plasma treatment followed by physio-absorption of PEG changed the surface from hydrophobic to hydrophilic. Prior to surface modification and during EF treatments, a layer of large bubbles covered the surface of the electrode

arrays (Figure 22, A). After PDMS surface modification, the bubbles formed during electrolysis were visually smaller, quickly coalescing and releasing from the electrode substrate (Figure 22, B. Without O_2 + PEG surface modification (Figure 22, A), at a voltage of 6 V, was initially about 330 mA but within minutes dropped to around 250 mA (Figure 23, A). For the same voltage (6 V) PCB electrodes with O_2 + PEG surface modification (Figure 22, B) sustained a stable current at 325-350 mA (Figure 23, B).

A. B.

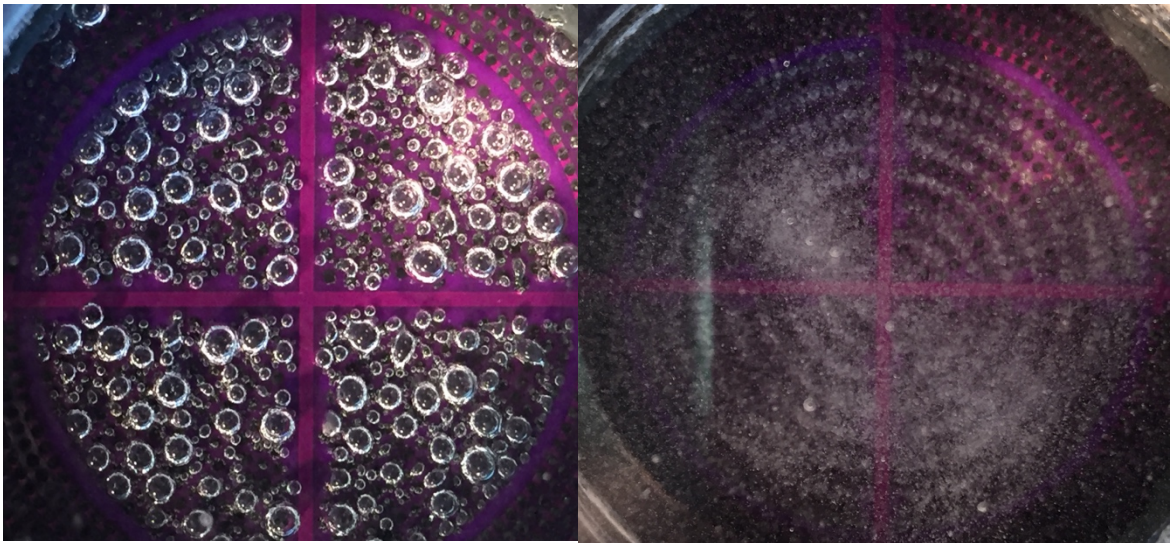

Figure 22. PDMS coated electrodes undergoing electrolysis +/- surface modification. (A) PDMS surface before surface modification. (B) PDMS surface after Oxygen Plasma Treatment + PEG grafting.

As previously mentioned, during constant current or constant voltage electrolysis, the wettability (hydrophobic/ hydrophilic properties) of the surface of an electrode will affect how long a bubble resides on the electrode. When a bubble resides on the surface of the electrode, especially when the diameter is large, the ohmic resistance to current across the electrode / electrolyte interface increases (Bouazaze et al. 2006). Figure 23 (A, B) depicts peaks or noise that

can likely be attributed to changes in electrolyte resistance as bubbles grow and detach. If we consider the 1st peak at 6 V for both before (Figure 23, A) and after (Figure 23, B) surface modification as the initial incremental resistance to current (R_0), it is not surprising that in both scenarios the current decreases from the initial peak as the electrolyte resistance increases for the same constant voltage. Although the surface modification was effective, the modified PDMS was not stable over multiple preliminary trials and unable to generate reproducible data and significant differences were observed between different electrodes. Furthermore, the flux and quantity of bubbles produced was much lower than achieved in the final electrode design.

A.

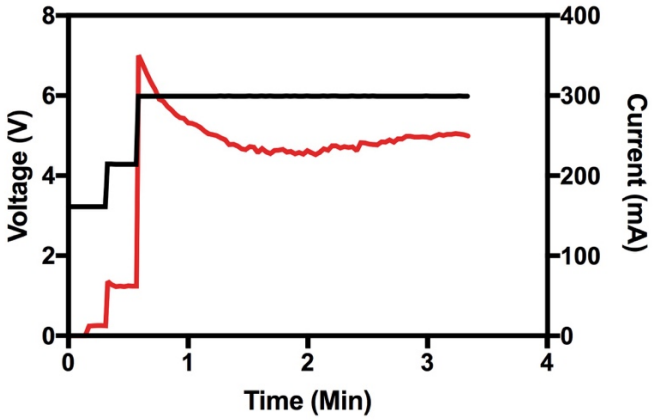

B.

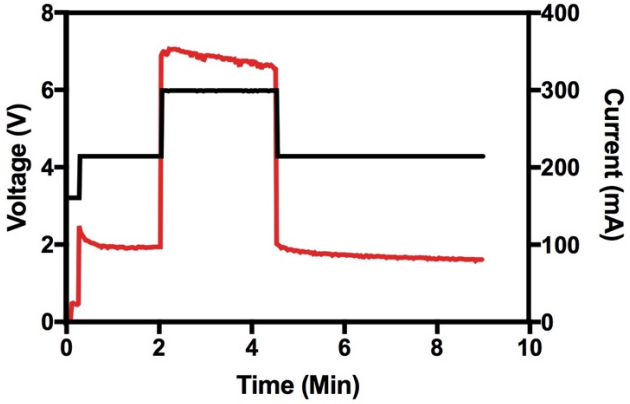

Figure 23. PDMS (+/- surface modification) current (mA) at different applied voltages. Current (mA) (red line) over time at varying voltage (V) (black line) of PDMS coated PCB electrodes before (A) and after (B) O_2 plasma surface modification + PEG grafting.

7.2 Titanium Coated Platinum Electrodes

TiPt electrode arrays were tested in HT and LT flotation conditions (n=3 for each condition). The microbubbles produced during electrolysis (Figure 24) were uniformly distributed and the flux was noticeably sensitive to changes in current.

Figure 24. Microbubbles produced by TiPt electrodes during EF.

For example, LT conditions generated a columnar pillar of upwardly rising bubbles without mixing. For HT flotation conditions, a larger current was constantly applied, and significantly more bubbles were produced. Using the current control feature, for both HT (Figure 25, A) and LT (Figure 25, B) conditions, a constant current of 300 mA and 600 mA respectively was applied for 20 minutes. The current was regulated in software by adjusting the applied voltage up or down based on "errors" the measured current value relative to the desired value. Limitations in the resolution of the custom implemented adjustable regulator resulted in oscillations in applied voltage and current around the set-point current (Figure 25), though these oscillations did not produce noticeable oscillations in the bubble flux or bubble behavior. No signs of corrosion were observed during the initial 3 experimental replicates for each condition. The electrodes have run EF treatments over 100 times subsequent to the preliminary experiments reported here, and have reproduced stable electrochemical readings over time without any apparent signs of corrosion.

A.

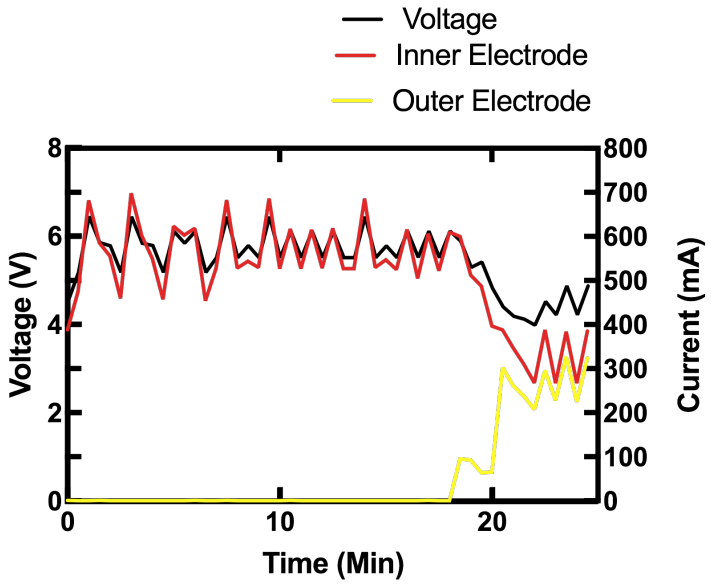

B.

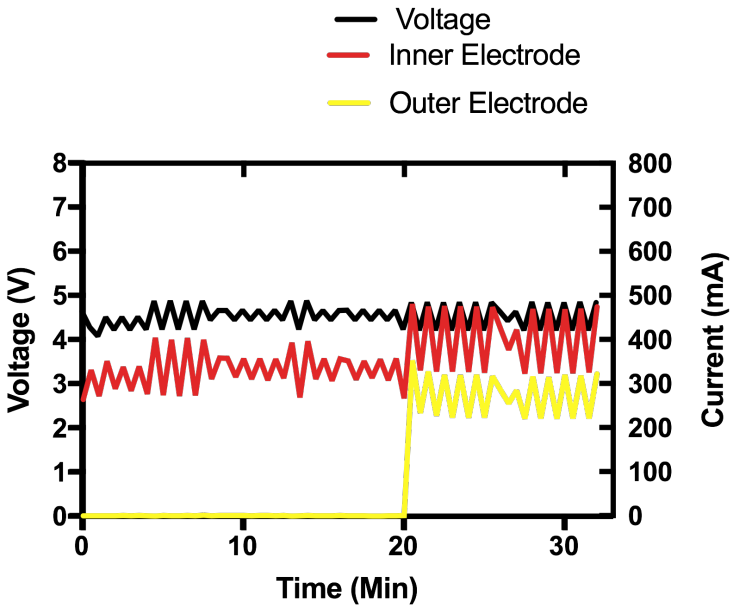

Figure 25. Current/ Voltage readings of TiPt electrodes during EF. Recorded current (mA) for high turbulence (A) and low turbulence (B) 20 minute EF treatments using TiPt electrodes.

7.3 LAMP ASSAY

7.3.1 Evaluation of Modified LAMP Primer Set

The modified primer set EcolC 3109_1 was quantitatively compared to the original primer EcolC 3109_0 with purified *E. coli* DNA over a range of DNA concentrations equivalent to 10^1 to 10^7 copy numbers per reaction (Figure 26). Applying a semi-logarithmic regression to the quantitative comparison model, significant differences between y-intercept values were observed ($P<0.001$) between the primer sets, with EcolC 3109_1 ($y_{int}=20.24$) reactions consistently amplifying sooner than those with the EcolC 3109_0 ($y_{int} = 31.88$) primer set. The detection limit for EcolC 3109_0 was 10^2 DNA copies, while EcolC 3109_1 was able to detect DNA present at 10^1 copy numbers at $t_T = 18$ minutes. These results confirm that modifications to the previously published LAMP assay (Teh et al. 2014) resulted in improved detection limits and more robust amplification.

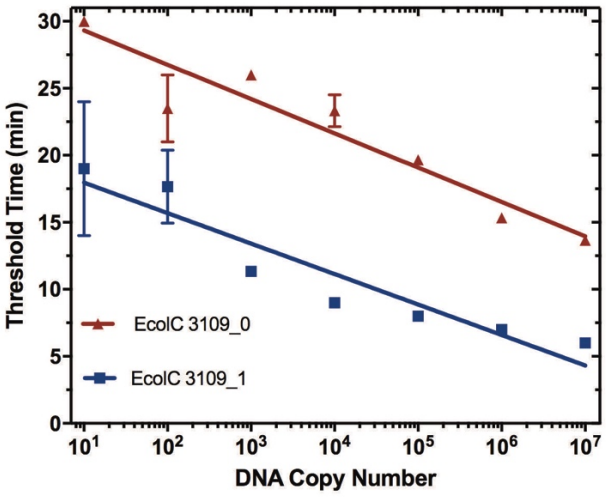

Figure 26. Performance of original versus modified EcolC 3109 LAMP primers. Quantitative comparison of observed threshold times for original primer set EcolC 3109_0 and modified primer set EcolC 3109_1 using purified *E. coli 25922* DNA.

7.3.2 Specificity of Modified EcolC 3109_1 Primer Set

In silico analysis supported specificity of the modified primer set (EcolC 3109_1) towards generic *E coli.* Primer set 3109_1 was 100% identical to 25 *E. coli s*equences including *E. coli* ATCC 29522 while the remaining 33 *E. coli* sequences evaluated shared ≥95% match identify between the glycerate kinase gene region and 3109_1 primer binding regions. Primer set 3109_1 showed little to no specificity towards non-E. *coli* strains with a mean query coverage of 15+/-21.7 %. A list of *E. coli* strains and non-*E. coli* strains with % match identity % query coverage respectively can be found in Appendix Table A1.

7.4 LAMP Performance for Detection of *E. coli* w/out EF Treatment

Representative amplification curves for control reactions using primer set EcolC 3109_1 with untreated cell suspensions are shown in Figure 27. The detection limit, where at least 95% of samples could be reliably detected, was observed to be about 10^5 CFU/mL, as 100% of samples at this concentration resulted in amplification, but only 48% of samples at 10^4 CFU/mL resulted in amplification. Mean threshold times observed in the positive 10^4 CFU / mL samples was 16.58 +/-3.43 minutes. Although EcolC 3109_1 detected purified *E. coli* DNA in quantities reliably at concentration as low as 10^2 DNA copy number (Figure 9), the detection limit was higher (equivalent to 500 CFU or genome copies) in samples where only crude lysis was used to expose genomic DNA. No positive detection was observed in a total of 54 assays of untreated samples at either concentration of 10^2 or 10^3 CFU/mL. The baseline performance of the assay on crude cell lysates assay (Figure 27) identified detection limitations and all subsequent electroflotation experiments were conducted with sample concentrations ≤ detection threshold limit = 10^5 CFU/mL ranging from 10^2-10^4 CFU/mL.

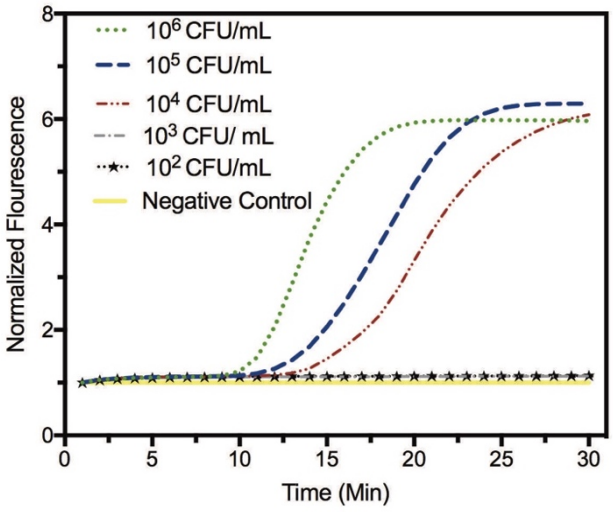

Figure 27. Representative LAMP curves at varying untreated E. coli 25922 concentrations (10^2-10^6 CFU/mL). The lowest detectable concentration in these untreated controls was 10^4 CFU/ml, though 10^5 CFU/mL is required for reliable detection.

7.5 Electroflotation Treatment (EF)

7.5.1 Evaluation of EF Treatment Effects on Detection Limits of *E.coli*

Samples were inoculated with varying concentrations of *E. coli 25922* and subjected to various EF treatment conditions. Significant effects of EF treatments on detection rates of LAMP were observed for both high turbulence (Figure 28A) (P=0.0019) and low turbulence conditions (P=0.002) (Figure 28C) at the low concentrations tested (10^3 and 10^2 CFU/mL). Using Dunnett's multiple comparison post-hoc analysis, 5 sets of experimental conditions at concentrations below 10^4 CFU/mL were observed to have significant differences in detection rates after EF treatment when compared to the corresponding controls. For high turbulence conditions, significant differences were observed for 10^2 CFU/mL at 15 minutes, 10^3 CFU/mL at 10 minutes, and 10^3 CFU/mL at 15 minutes of EF treatment with a mean detection rates of 18.57% (P=0.009), 11.11% (P=0.0031), 11.11% (P=0.0031) respectively (Figure 28B). For low turbulence treatments in

samples containing 10^3 CFU/mL, significant differences were seen in 15 minutes (P=0.0007) and 20 minutes (P=0.0371) of EF treatment with mean detection rates of 40.73% and 25.92% respectively (Figure 28D). Low turbulence conditions had overall higher detection rates for both 10^3 and 10^4 CFU/mL samples for both 15 and 20 minutes EF treatment when compared to their high turbulence counterparts. Although not considered significant, 100 % detection was achieved in 1 experimental replicate for both 10 and 15 minutes for 10^4 CFU/mL under low turbulence conditions. Similarly, over 50% detection rates were achieved for some 2 experiments at 10^3 CFU/mL. Although detection rates did improve for conditions previously described, reliable detection requires 95% detection of positive samples.

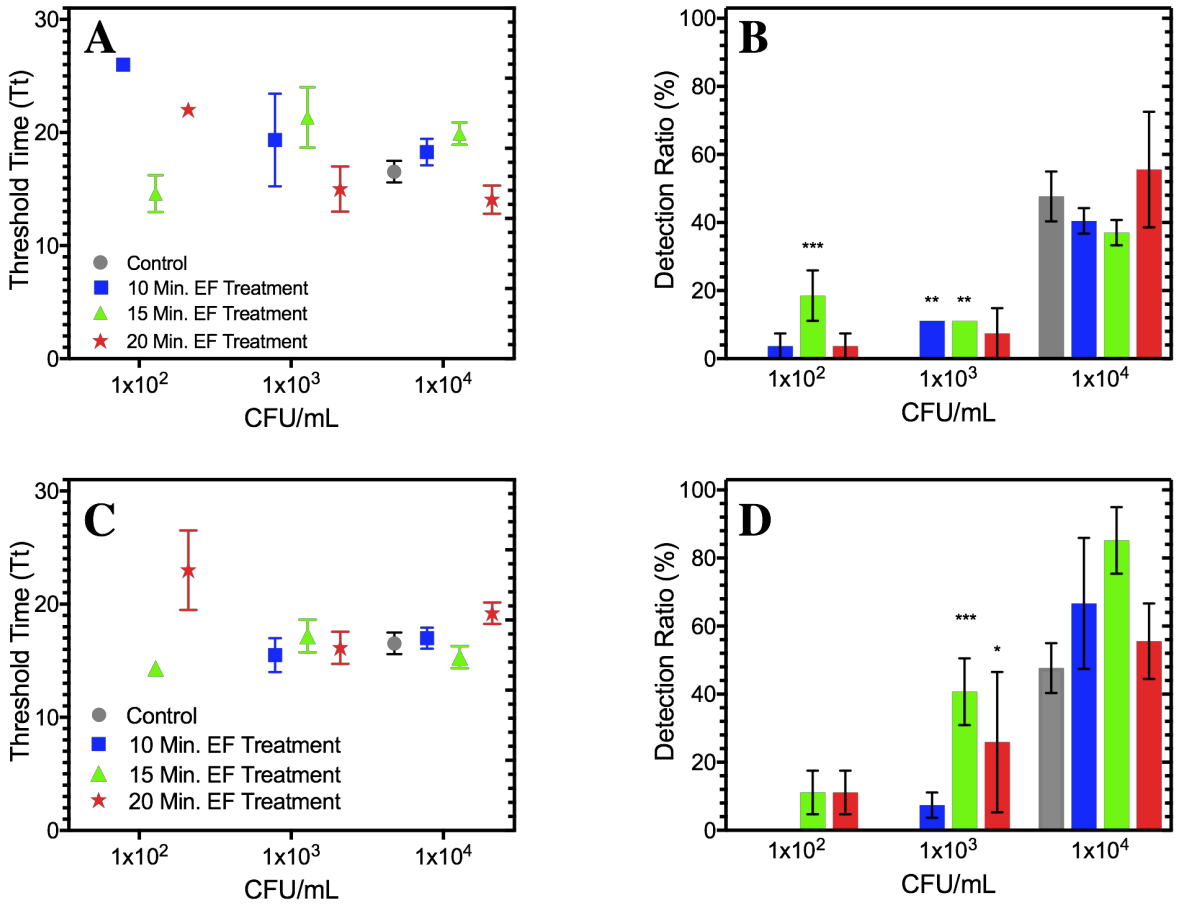

Figure 28. Sensitivity of LAMP assay after high (B) and low turbulence (D) Electroflotation treatments. In (B; high turbulence) and (D; low turbulence) each data point represents the detection ratio from 27 assays conducted on samples from one replicated electroflotation treatment (n=3 for each treatment). Treatments significantly different than controls are designated with asterisks (*p<0.05, **p<0.01, ***p<0.001) Error bars are standard errors of the means.

7.5.2 Detection Rate Distribution Between Collected Fractions

The distribution of *E. coli* detection in each 1mL fraction collected after EF treatment was analyzed by conducting 3 LAMP assays/1mL fraction to determine the degree of stratification of *E. coli* in the top fractions of the media, and to observe which treatments were most effective at concentrating bacteria near the surface (Figure 29). Significant differences were observed ($P < 0.0001$) in detection rates between fractions 1, 2 and 3 only for high turbulence treated samples at

20 minutes (Figure 29C) while low turbulence treated samples showed no *overall* difference in detection rates between fractions. EF conditions that resulted in highly variable detection rates between fractions 1, 2 and 3, did not correspond, or share overlap with, the conditions where increased or improved detection rates with EF treatments were observed. Generally, low turbulence conditions had more even distribution of detection rates between fractions 1,2 and 3 for all concentrations (CFU/mL) and varying durations (10,15,20 minutes) of EF treatment when no chemical additives were added to the buffer to promote flocculation or to mask the hydrophobicity of cell surfaces.

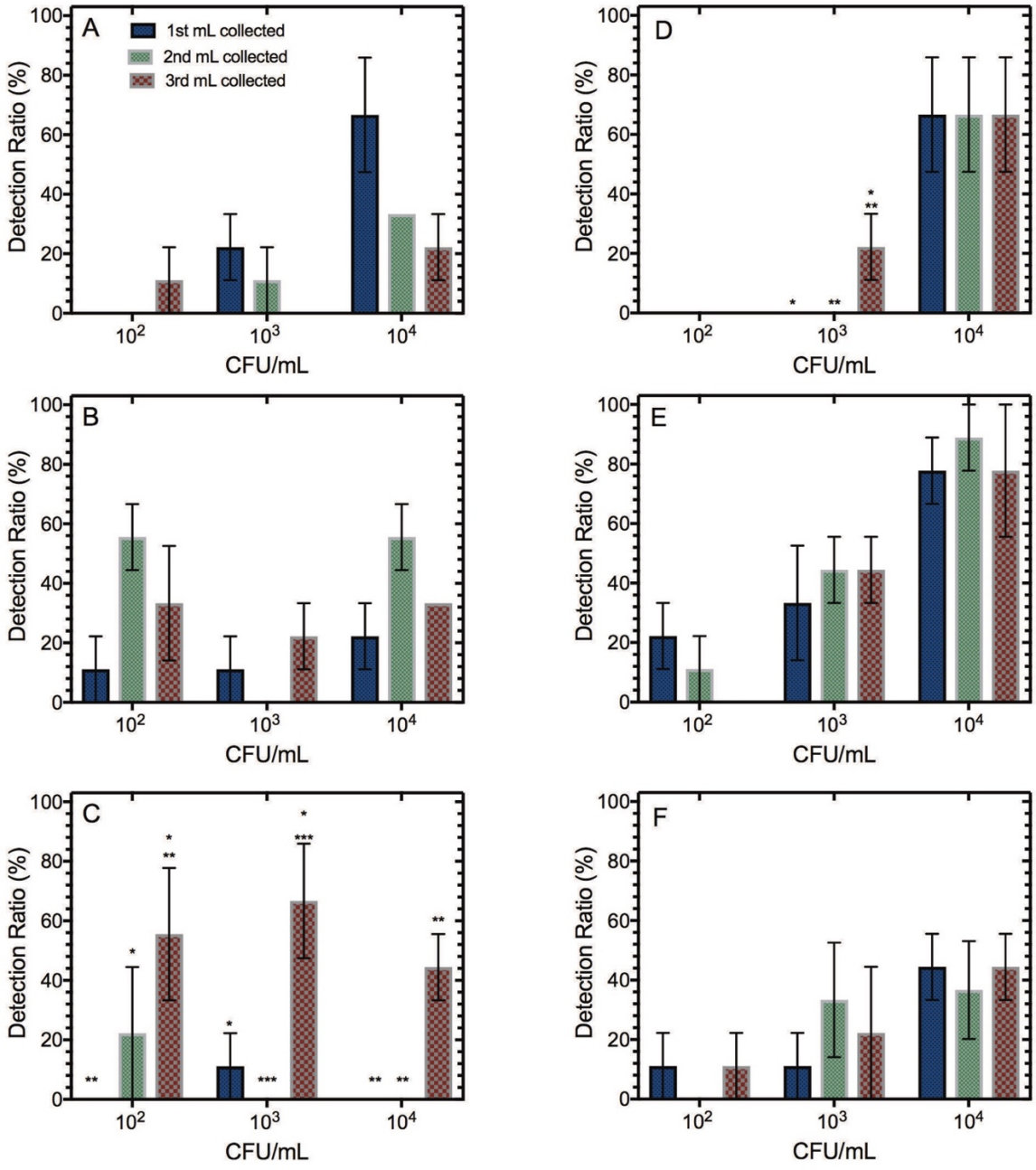

Figure 29. Distribution of positive LAMP assay detection in individual collected fractions. 3 LAMP assays were performed for each 1st, 2nd, and 3rd mL sample fractions collected following high turbulence conditions for 10 (A), 15 (B), and 20 (C) minute EF treatment and low turbulence conditions for 10 (D), 15 (E), and 20 (F) minute EF treatment. Detection ratios are percentages of positive detection out of 3 assays for each recovered fraction. Each EF treatment for each bacterial concentration (10^2-10^4 CFU/mL) was repeated 3 times. Error bars are standard errors of the means.

7.6 Pluronic F-68 Inhibition on LAMP

LAMP assays were not inhibited by the addition of pluronic to samples at all tested concentrations (0.05%, 0.1%, 0.5%, 1.0%, and 2.0 %) (Figure 30). Inhibition on LAMP, characterized by increased threshold times, was evaluated by linear regression. The linear regression between threshold time and pluronic concentration (Y= 0.01735*X+ 12.93) had a slope that was not statistically different than showed zero, (p=0.9542) indicating no observable effect of pluronic concentration.

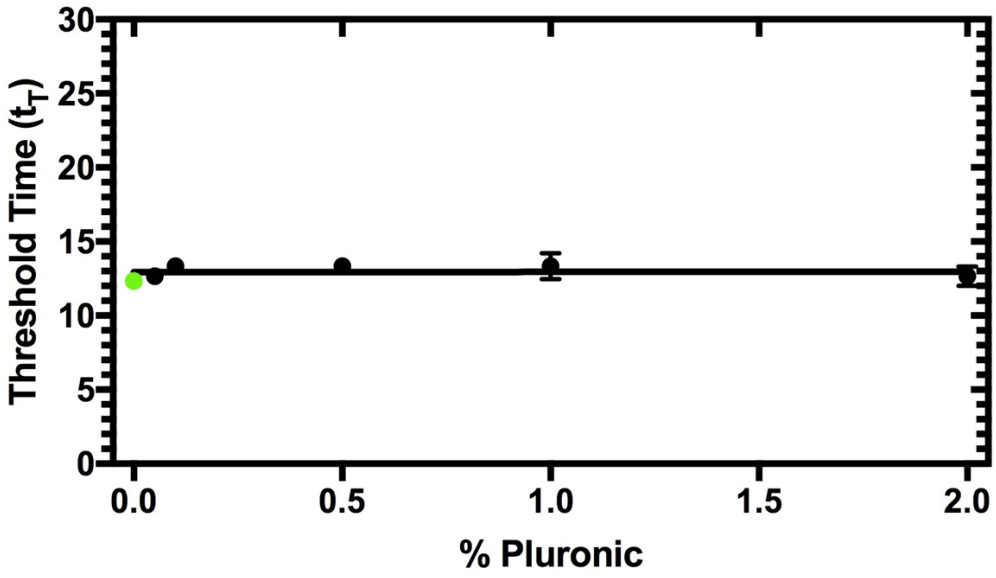

Figure 30. Inhibition on LAMP assays by Pluronic. Observed LAMP threshold times for samples containing varying concentrations of pluronic (0.0%, 0.05%, 0.1%, 0.5%, 1.0%, 2.0 %). Control group (0% pluronic) indicated by green dot. Each data point represents 3 replicates at each condition. Error bars are standard errors of the mean.

7.7 Chitosan Inhibition on LAMP

The effects of chitosan in a LAMP assay reaction were evaluated. Significant effects on threshold times (t_T) of varying chitosan concentrations were observed (p= 0.0001). Complete

inhibition of LAMP occurred from samples containing chitosan concentrations above $5x10^{-4}$ g mL^{-1}. This resulted in and no detection of *E.coli 25922* by LAMP under these conditions. Using Dunnett's multiple comparison post-hoc analysis, 5 chitosan concentrations were observed to have significant effects on LAMP when compared to a corresponding control assay containing no chitosan (t_T=9 min., n=3). For chitosan concentrations above 10^{-7} g L^{-1} significant differences in mean threshold times were observed for 10^{-6} g mL^{-1}, 10^{-5} g mL^{-1}, 10^{-4} g mL^{-1} with mean threshold times of 11.33 (p=0.04), 16.67 (p=0.0001) and 21 (p=0.0001) respectively (Fig. 31).

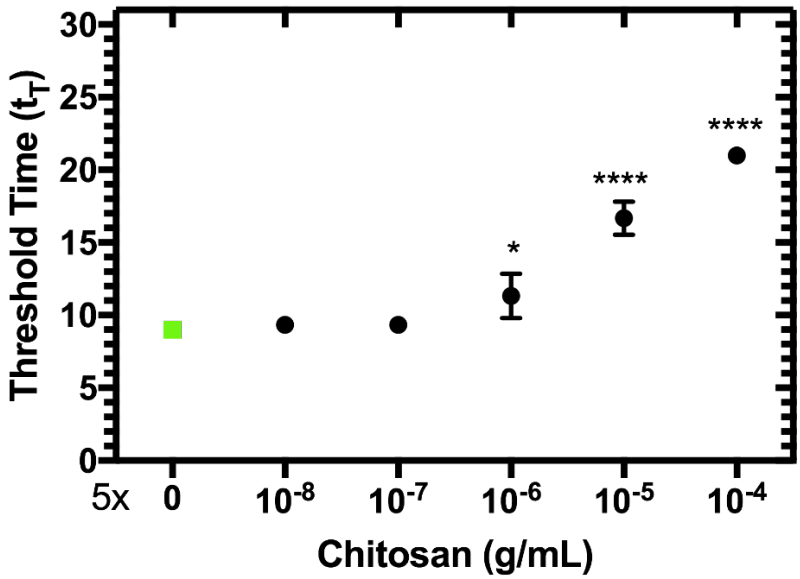

Figure 31. Inhibition on LAMP assays by chitosan. Observed LAMP threshold times for EF samples containing varying concentrations of chitosan (0, $5x10^{-8}$, $5x10^{-7}$, $5x10^{-6}$, $5x10^{-5}$, $5x10^{-4}$, $5x10^{-3}$ g L^{-1}). Chitosan completely inhibited LAMP at concentration > 10^{-3} g L^{-1} (data not shown). Each data point represents the mean threshold time (t_T) from (n=3) LAMP assays. Treatments significantly different than control (0 g L^{-1} chitosan, green dot) are indicated by asterisk (*p<0.05, ****p<0.0001) Error bars are standard errors of the mean.

7.7.1 Preventing LAMP Inhibition by Chitosan

The amino group of chitosan is cationic below its pKa (~pH 9.5). In this state, it will bind through electrostatic interaction to negatively charged negatively charged bacterial cells i.e. *E. coli* and also anionic DNA. Chitosan binding to anionic DNA can also prevent LAMP primer binding and inhibit amplification. At pH 6 chitosan present in concentrations of 0.01 and 0.1 g L^{-1} inhibited amplification of 0.2 ng of *E. coli 25922*. LAMP was not inhibited, however, for the same concentrations of chitosan (0.01, 0.1 g L^{-1}) at pH 10 (Figure 32). Although PCR reactions can be completely inhibited at pH > 9.0, LAMP assays with a sample pH 10 without chitosan, were only slightly inhibited and still robust enough to be able to amplify template DNA. The time to detection was longer by 3 minutes when comparing threshold times from the pH 10 chitosan (0.01, 0.1 g L^{-1}) samples (t_T=15 min.), to control samples (t_T=12 min.). No difference in threshold time (t_T) was observed between samples containing 0.01 or 0.1 g L^{-1} chitosan. By adjusting the pH of the samples from pH 6 to pH 10, LAMP inhibition by chitosan was prevented and amplification of target was unaffected.

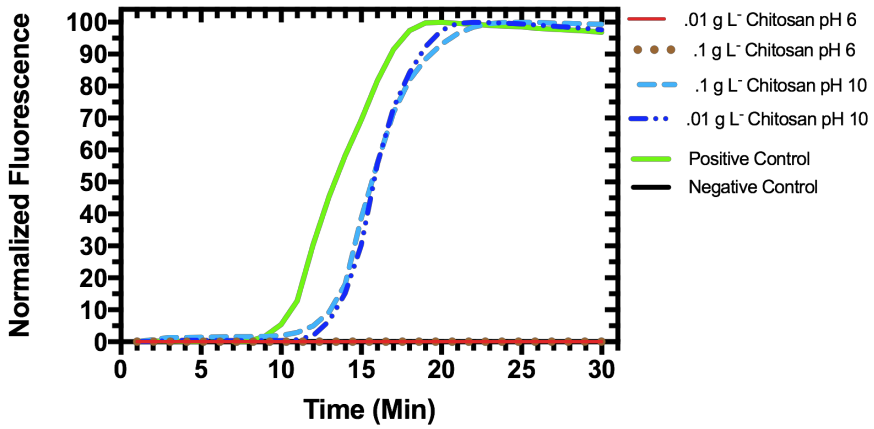

Figure 32. Increasing sample pH to prevent LAMP inhibition by chitosan. Representative LAMP amplification curves for samples (pH 6 and pH 10) containing 0.01 and 0.1 g L^{-1} chitosan. Samples (pH 6) containing 0.01 and 0.1 g L^{-1} chitosan completely inhibited LAMP. Whereas samples adjusted with NaOH to achieve pH 10 also containing 0.01 and 0.1 g L^{-1} chitosan did not inhibit LAMP. All reactions contained 0.2 ng *E. coli 25922* DNA except the negative control. 3 replicate assays were performed for each condition.

7.8 EF treatment +/- Pluronic F-68

To protect cells from lysis by hydrodynamic shear forces during EF treatments, varying concentration of pluronic (0.001, 0.01, 0.1, 1.0 g L^{-1}) were added to EF samples. In preliminary experiments (data not shown) 0.001 g L^{-1} pluronic concentration was presumed too low to affect EF treatments and did not significantly change the detection rates by LAMP. At the same time, the addition of 1 g L^{-1} pluronic to EF treatments resulted in undesirable amounts of foam formation during electrolysis, leading to premature sample displacement and potential aerosolization of the target pathogen. Therefore, after preliminary screening of pluronic concentrations, 0.1 and 0.01 g L^{-1} were subsequently investigated.

Using a 2-way ANOVA, no significant effects on LAMP detection rates were observed for 15 minute HT with the addition of pluronic (0.01, 0.1 g L^{-1}) (Figure 33B) when compared to control samples subjected to EF but without pluronic. However, using Tukey's multiple comparison pot-

hoc analysis, 2 experimental conditions were observed to have significant effects on LAMP detection rates after EF treatment when compared to corresponding controls (Figure 30D). For 15 minute HT conditions, significant differences were observed for 10^3 CFU/mL at 0.01 g L^{-1} ($p=0.04$) and 0.1 g L^{-1} ($p=0.019$) with a mean detection rate of 55.55% and 62.96% respectively (Fig. 33 B). In parallel, significant effects of EF treatments with the addition of pluronic (0.01, 0.1 g L^{-1}) on LAMP detection rates were observed for 20-minute LT ($p=0.0059$) conditions at 10^2 and 10^3 CFU/mL tested concentrations (Fig. 30 D). Using Tukey's multiple comparison post-hoc analysis, 2 experimental conditions were observed to have significant effects on LAMP detection rates after EF treatment when compared to corresponding controls. For 20-minute LT conditions, significant differences were observed for 10^3 CFU/mL at 0.01 g L^{-1} ($p=0.0016$) and 0.1 g L^{-1} ($p=0.0006$) with a mean detection rate of 85.18% and 92.59% respectively. No significant differences were observed between different pluronic concentrations (0.01, 0.1 g L^{-1}) at either tested *E. coli* concentration (10^2, 10^3 CFU/mL).

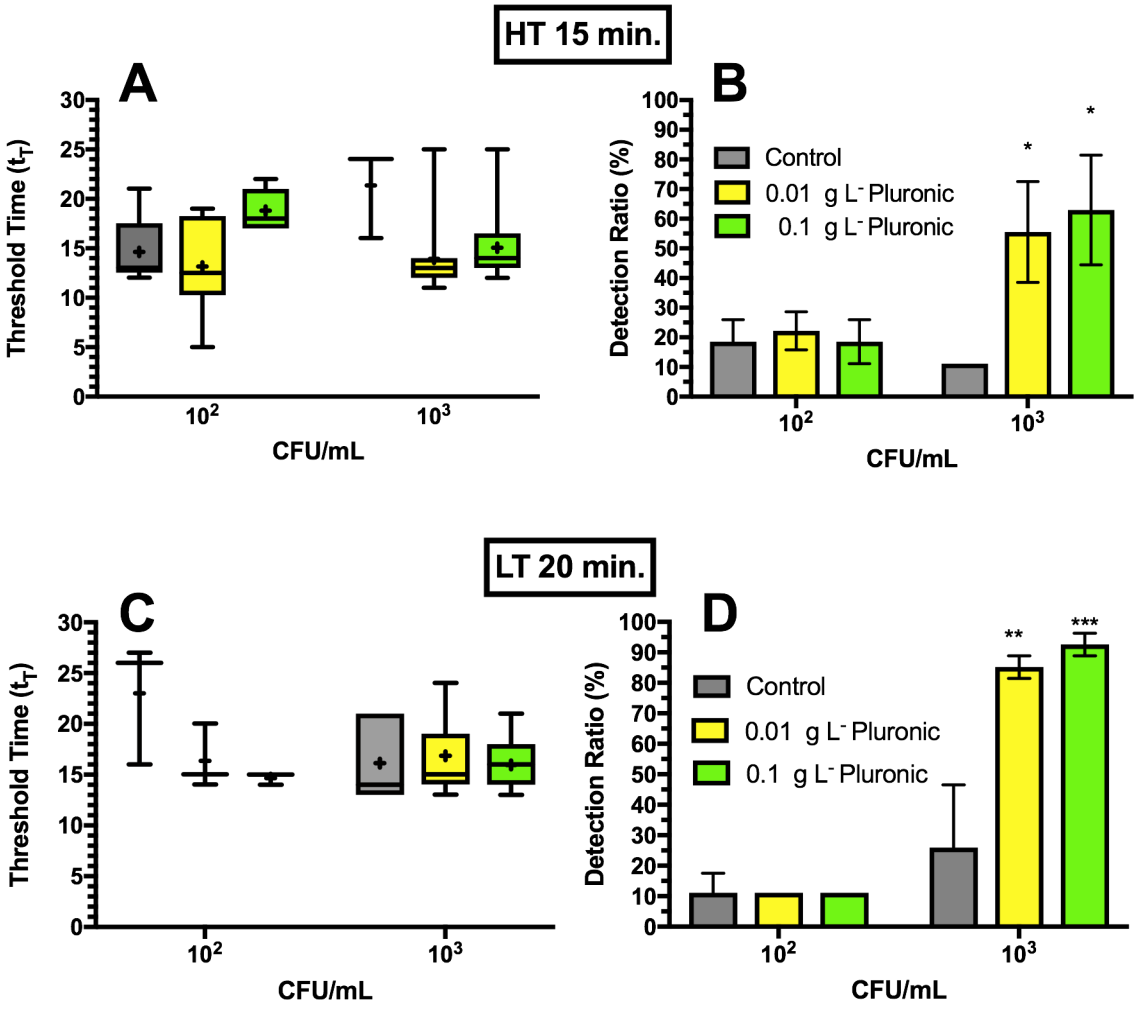

Figure 33. Sensitivity of LAMP assay with EF +/- pluronic F-68 treated samples. LAMP threshold times after 15 min. HT (A) or 20 min LT (C) with the addition of 0.01 and 0.1 g L^{-1} pluronic to EF treatments. In (B) and (D), each bar represents the mean detection ratio from 27 assays conducted on samples from 3 replicated EF treatments. (9 assays/ treatment, n=3 for each treatment). Treatments significantly different than controls are designated with asterisks (*p<0.05, **p<0.01, ***p<0.001). In (B) and (D) Error bars are standard errors of the means. For (A) and (C), whiskers are from min to max and means are indicated by +. The box extends from the 25th to 75th percentiles.

Using a 2-way ANOVA, no significant effects on LAMP detection rates were observed for 15 minute HT with the addition of pluronic (0.01, 0.1 g L^{-1}) (Figure 33B). However, using Tukey's multiple comparison post-hoc analysis, 2 experimental conditions were observed to have significant effects on LAMP detection rates after EF treatment when compared to corresponding

controls (Figure 33D). For 15 minute HT conditions, significant differences were observed for 10^3 CFU/mL at 0.01 g L^{-1} ($p=0.04$) and 0.1 g L^{-1} ($p=0.019$) with a mean detection rate of 55.55% and 62.96% respectively (Figure 33B).

In parallel, significant effects of EF treatments with the addition of pluronic (0.01, 0.1 g L^{-1}) on LAMP detection rates were observed for 20-minute LT ($p=0.0059$) conditions at 10^2 and 10^3 CFU/mL tested concentrations (Figure 33D). Using Tukey's multiple comparison post-hoc analysis, 2 experimental conditions were observed to have significant effects on LAMP detection rates after EF treatment when compared to corresponding controls. For 20-minute LT conditions, significant differences were observed for 10^3 CFU/mL at 0.01 g L^{-1} ($p=0.0016$) and 0.1 g L^{-1} ($p=0.0006$) with a mean detection rate of 85.18% and 92.59% respectively. No significant differences were observed between different pluronic concentrations (0.01, 0.1 g L^{-1}) between tested *E. coli* concentration 10^2 CFU/mL.

Low turbulence conditions had overall greater increased detection rates by LAMP than compared to corresponding high turbulence conditions at 10^2 CFU/mL and 10^3 CFU/mL when media was supplemented with pluronic. Furthermore, the addition 0.1 g L^{-1} pluronic resulted in greater increases in detection rates compared to the addition of 0.01 g L^{-1} pluronic for tested concentrations of 10^3 CFU/mL for both high and low turbulence conditions. LT turbulence conditions may be more desirable to stably recover aggregate flocs of bacteria by chitosan, therefore the concentration of pluronic that performed the best under LT conditions (0.1 g L^{-1}) was chosen for subsequent EF treatments to test the effects of chitosan. In summary, reliable detection (≥95%) was almost achieved (92.59%) for 20-minute LT EF treatments testing bacterial quantities of 10^3 CFU/mL with the addition of 0.1 g L^{-1} pluronic. While this is not quite the 95% detection rate required for low tolerance pathogens, this is significant improvement from the ~25% detection

rates that were observed in corresponding controls without pluronic. In subsequent experiments, to investigate the effects of chitosan, EF treatments were conducted only on samples containing 10^2 CFU/mL and 0.1 g L^{-1} pluronic at 20-minute LT EF conditions.

7.9 EF treatment +/- (Chitosan + Pluronic)

LAMP was conducted on the first mL collected after 20-minute low turbulence EF treatments containing 10^2 CFU/mL bacterial quantities and 0.1 g L^{-1} pluronic and 0.1 and 0.01 g L^{-1} chitosan. Significant differences were observed for treatments containing chitosan ($p=0.0001$) when compared to corresponding controls (Figure 34). Dunnett's multiple comparison post-hoc analysis identified 2 treatments that were significantly different from the EF treatments only containing pluronic and no chitosan. For 10^2 CFU/mL LT 20 min, when compared to corresponding treatments only containing pluronic, significant differences were observed for EF treatments containing 0.01 g L^{-1} chitosan ($p=<0.0001$) and 0.1 g L^{-1} chitosan ($p=<0.0001$) with mean detection rates of 96.3% and 100% respectively.

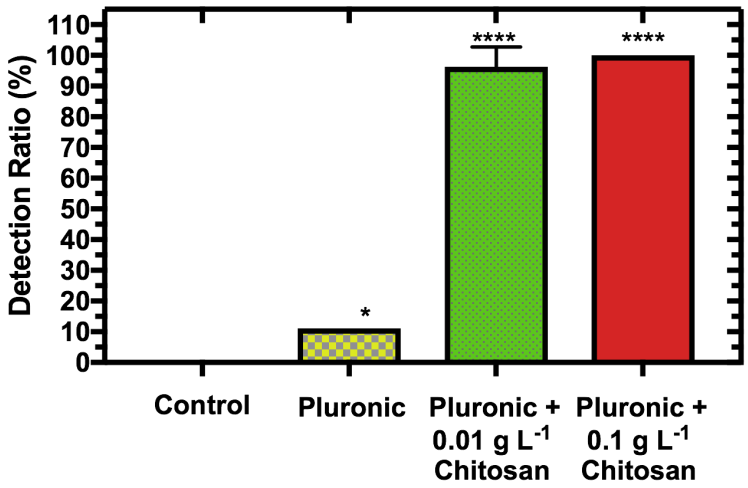

Figure 34. LAMP assay detection rate of EF +/- (chitosan + pluronic F-68). 10^2 CFU/mL, Low turbulence, 20-minute treatment with the additions of 0.1 g L^{-1} pluronic + 0.01 g L^{-1} chitosan. Control contained no pluronic. Each bar represents the total detection rate from 9 assays testing only the 1st mL collected from 3 replicated EF treatments (3 assays/ 1 mL, n=3). Treatments significantly different than controls are designated with asterisk (*$p<0.05$, ****$p<0.0001$). Error bars are standard errors of the means.

8. DISCUSSION

8.1 Electrode Arrays

The feasibility and efficacy of the electroflotation system relies largely on electrode arrays to stably support electrolysis reactions in a highly corrosive environment without material degradation (*i.e.,* anodic corrosion) and material property changes (*i.e.* decreased surface conductivity). Platinum coated titanium electrode arrays demonstrated superior performance during electroflotation treatments without any signs of corrosion and supported stable current densities without any additional protective coating or surface modifications. Conductive PDMS, carbon conductive paste, and silver filled epoxy were evaluated with electrochemical tests, SEM, and EDS as corrosion resistant coatings to protect exposed electrode metal on custom PCB electrode arrays. While conductive coatings work for industrial applications like creating electrical

pathways, or as stand-alone electrodes, none of the tested corrosion inhibiting coatings were capable of long term corrosion protection for electroflotation treatment conditions. The manufacturing costs of platinum coated titanium electrode arrays are more expensive ($33.00 per unit) when compared to PCB electrode arrays ($11.00 per unit), but last longer and do not require additional costs and labor to perform post processing steps *i.e.,* screen printing corrosion inhibiting coatings. Innovations in production and development of electrochemical industrial titanium anodes supports prototyping applications when low cost and low volume manufacturing are necessary. Advances in technology that allow normally large scaled industrial products to be scaled down while remaining feasible demonstrates a promising future between industry and university research.

8.2 Foundational Electroflotation Experiments

In order to increase the likelihood of detection of nucleic acid amplification model LAMP, this research introduces a novel technology to extract and concentrate small quantities of bacteria dispersed in ecological-scale samples using a portable, automated, self-contained electroflotation system. Even with the EF treatment however, detection rates at these concentrations were far below reliable detection rates (*i.e.,* 95%) generally expected for a practical diagnostic system. However, findings presented in these foundational experiments suggest the efficacy of electroflotation treatment may be significantly improved through use of different chemical additives to improve aggregation or resistance of bacteria to shear, or different electrolysis conditions. We were surprised too in this case that the electroflotation method recovered and concentrated culturable bacteria directly from a simple buffer system (unpublished data).

8.3 Effect of Pluronic on Electroflotation

The addition of a non-ionic surfactant (Pluronic® F-68) to EF treatments improved concentration of *E. coli* 25922 and therefore improved detection rates of *E. coli 25922* by LAMP. The most impressive effect of adding pluronic to EF samples, observed for the addition 0.1 g L^{-1} pluronic F-68 to 10^3 CFU/mL bacterial quantities and subjected to 20 minutes low turbulence EF treatment, increased detection rates from 25% to 92.59%.

The mechanism by which pluronic F-68 improves concentration of dispersed bacteria during flotation was not investigated. Interestingly, one study reports the use of surfactants to improve electrokinetic stability of electrodes in lab-on-chip microdevice by promoting smaller bubble diameters and also more rapid bubble detachment from the electrode surface (Lee, H.Y., Barber, C., Minerick 2014). While this effect was not measured directly, visual observation confirmed that larger bubbles sporadically detaching from electrodes occurred less frequent. This suggests that the effect of pluronic to improve concentration of bacteria by EF extends beyond bubble-particle interactions by enabling quicker bubble detachment likely resulting in overall smaller and more uniformly sized microbubbles.

Pluronic F-68 is a non-ionic surfactant added to cell cultures to reduce shear forces and also reduce bacteria attachment to glass. Surfactants modify the surface tension forces that typically attract, stress or disperse biomaterial are commonly added to bioreactors to aerate cell cultures and protect cells from shear forces that result in cell lysis and death (Walls et al. 2014). The exact molecular mechanism by which Pluronic F-68 protects cells but it is unknown, but believed to be attributed to Pluronic F-68 masking the hydrophobic properties of the cell membrane. By design, surfactants interplay with bubbles result in local gradient changes in surface tension on the bubble surface so that a bubble will slide passed a cell with lowered interactions

and collision efficiency (Walls et al. 2014). Theoretically, this should prevent bubble-cell attachment and decrease flotation efficiency. In contrast, Pluronic F-68 significantly improved EF concentration efficiency. Pluronic F-68 is an amphiphilic molecule that can self-assemble into microstructure micelles (Farías et al. 2009). Surfactant micelles can encapsulate other molecules and has been used widely for the solubilization of drugs and drug delivery (Fan et al. 2012). Similarly, it is conceivable pluronic micelles formed around detectable cell material (*i.e.,* free DNA, lipids, cell fragments) during EF treatments. The observed increased detection rates by LAMP may be attributed to the concentration of detectable cell material otherwise not observed in corresponding EF treatments without pluronic.

8.4 Chitosan, Flocculation and Effects on Electroflotation

Chitosan was added to electroflotation treatments to support aggregation of dispersed bacteria, which can result in substantial increase in particle (*i.e.,* bacteria) quantity recovered. Research using chitosan as a bacterial flocculation agent for *E.coli* suspensions of 10^9 CFU/mL suggests that optimal concentrations occur between 20-80 mg/g of cell dry weight depending on other factors like pH and degree of chitosan polymerization (Strand et al. 2001). Predicting adequate chitosan concentrations based on the dry weight of cells is impractical when conducting EF on environmental samples containing unknown quantities of dispersed bacteria at low titres ($<10^2$ CFU/mL). In other reports optimal chitosan or polymer concentration was found to be 10-20 μg/ billion cells, 25-75 g/L (Pearson et al. 2004), 20mg/ g of *chlorella* (Zhou et al. 2016) It is generally agreed that small increases or decreases in polymer dosage can have a large affect on the stabilization of the dispersed system and significantly affect the absorption rates of the flocculant to the substrate, however there is a lack of agreement on specific optimal chitosan concentrations

reported in literature. This can be partially attributed to the challenges and complexity of quantifying properties of a dispersed colloidal system including the disagreement about the fundamental mechanism by which chitosan binds suspended solids; by bridging (Yang et al. 2012) or by charge neutralization (Barany and Szepesszentgyörgyi 2004).

To my knowledge, chitosan has previously been used to flocculate large quantities of bacteria ranging from 10^7 – 10^9 CFU/mL. This is up to 7 orders of magnitude greater than the bacterial concentrations used in EF treatments (10^2-10^4 CFU/mL). To increase the likelihood of chitosan interacting with dilute suspension of bacteria, a relatively large dose of chitosan proportional to bacteria was added to EF treatments. For EF treatments containing ~10^2 CFU/mL *E.coli*, 0.01 or 0.1 g L^{-1} was added to flocculate ~ 38,000 bacterial cells (the approximate quantity of 10^2 CFU/mL cells dispersed in 380 mL of media).

Adding chitosan in large concentrations may have other benefits as well. Firstly, by the common "jar test method" 10^9 CFU/mL cell suspensions and chitosan incubate together as a stationary culture for 24 hours during which cells are removed via sedimentation (Strand et al. 2003). Predictively, flotation would counteract any flocculation achieved by sedimentation and therefore a larger dosage of chitosan may be required for optimal flocculation. Secondly, chitosan has lower solubility in tested EF media (0.1 M potassium phosphate buffer) due to the presence of buffering salts that bind to chitosan counterions (anions) resulting in charge neutralization (Kong et al. 2010). Reduced solubility may decrease chitosan interactions with bacteria, and therefore a larger dosage of chitosan may be required for optimal flocculation. Thirdly, to maintain EF treatments a rapid process, the incubation period with chitosan restricted to 20 minutes. This incubation time is much shorter than previous studies (> 2 hours) using chitosan as a flocculant for biological materials and therefore a larger dosage of chitosan may be required for optimal

flocculation. Finally, studies report using much larger cell concentrations and therefore a larger dosage of chitosan may be required for optimal flocculation. For these reasons combined, chitosan was used in concentrations of 0.1 g L^{-1} and 0.01 g L^{-1} totaling 0.038 g chitosan and 0.0038 g chitosan to flocculate approximately 38,000 cells.

8.4.1 Preventing LAMP Inhibition by Chitosan

Despite LAMP resiliency against many common inhibitors, chitosan significantly inhibited detection by LAMP. Polysaccharides commonly found in environmental samples and plant matter are notorious inhibitors of nucleic acid amplification like PCR and competitively bind to template DNA, DNA polymerases and primer binding sites, preventing the initiation of DNA amplification. Diluting the sample can lower the concentration of inhibitors, however, this method is impractical for this application because improved detection is realized by concentrating a sample, not diluting. Unfortunately, by design, inhibitors that have aggregated during flocculation may also be concentrated during EF treatments.

The addition of chitosan as a flocculant to EF treated samples completely inhibited LAMP assays at concentration greater than 5 x 10^{-4} mg/mL. At pH less than ~6.2 and below chitosan's pKa (~pH 9.5), chitosan has a strong positive charge and will bind strongly to negatively charged anions including template DNA inhibiting isothermal nucleic acid amplification. Our approach to prevent LAMP inhibition by chitosan was adapted from a method that successfully extracted DNA on microchips lined with chitosan coated silica beads (Cao et al. 2006) . In their system, when the buffer flowing through microchannels of the device was pH 5, DNA bound to chitosan coated beads, and then eluted from the beads at pH 10. This method was particularly desirable because it does not require downstream DNA purification or extraction methods to remove inhibitors. The

pH can be titrated in the same tube as the recovered EF sample. This aligns nicely with platforms like the BioRanger™ that has a heat block capable of lysing cells at 100°C so that all methodologies in this research, including DNA extraction, can be done in the field.

8.6 EF POC Testing Limitations & Future Work

The EF system potentiates diverse sample aquistion including irrigation water, agricultural product rinsate, drinking water, and waste water. However, the electroflotation treatment conditions used to achieve reliable detection of *E. coli* 25922 were carried out in a simple buffer system. It is therefore difficult to accurately assess the practical use of electroflotation as a viable sample preparation method without testing on *real* agricultural samples i.e. food and water. Sample preparation methods to extract pathogens from water will undoubtedly have different, and simpler, requirements than procedures to extract pathogens from milk, ground beef or agricultural rinsates. To apply the EF system in POC testing scenarios, different types of environmental samples need to be tested to establish custom process settings required to achieve detection of bacterial targets from unique sample matrices.

The EF experiments in this objective were conducted using a feedback loop to maintain a constant desired current (mA) during electrolysis (i.e. 300 mA and 600 mA). By controlling current we can generate consistent bubble flux for electroflotation in any media irrespective of the media conductivity. However, applying a sustained max potential (12 V) for long durations using EF sample media with low conductivity will result in electrode over-potential to a degree that was not measured in this study.

A single type of environmental sample matrix can contain many different bacterial strains and/or species and therefore can host and transmit numerous types disease causing pathogens. For

example, spinach products have been linked to outbreaks of *Listeria, Salmonella* and *E. coli*. A multiplexing LAMP assay that would allow simultaneous detection of all 3 bacterial strains in a single reaction tube would be ideal for agricultural samples processed by electroflotation, which indiscriminately concentrates and extracts any particles ranging from the size of 0.5 microns to 200 (*i.e.,* bacterial pathogens) present in the sample matrix. While PCR multiplexing technology is more developed, where multiple DNA targets can be identified, LAMP technology multiplexing assays are limited and complicated to design. The more primers that are added to a single LAMP assay the greater occurrence of interference due to variances in amplication efficiencies (Sahoo et al. 2016). Currently to identify pathogens by LAMP the user would have to know what pathogen is being targeted and have primers designed for the specific pathogen, and multiplexing alternatives relying on automated parallel reactions from the same sample are being developed. The application of electroflotation could be greatly expanded upon by research and development of LAMP multiplexing technology. The realization of this technology is not far in the distant future as new methods to improve LAMP multiplexing continue to evolve. By replacing the poly (T) region of the FIP primer with a target specific barcode by nicking endonuclease activity, researchers at the Nanjing University School of Medicine in China designed a four-plexed LAMP assay to detect hepatitis B virus, hepatitis C virus, human immunodeficiency virus, and *Treponema pallidum* in a single LAMP reaction tube (Liang et al. 2012). Our lab has designed primer regions targeting spectrally unique assimilating probes so that different targets can be distinguished, potentiating application for multiplexing technologies. LAMP is an ideal detection model for agricultural diagnostics, however improvements in multiplexing technology, that maintain sensitive and reliable detection, are required to realize the full potential of a POC sample acquisition by electroflotation.

8.7 Safety Concerns

During EF treatments, electrolytically produced hydrogen and oxygen gases are allowed to mix in the flotation chamber (vented to the atmosphere) and gas trap creating a potentially hazardous scenario. While the lack of ignition sources and small diameter of the solid steel ejection port make ignition of the mixture unlikely, we also conducted an analysis of the worst-case explosion risk within the EF cartridge. In this worst case scenario the maximum pressure within the vessel was estimated for the case of an instantaneous and complete combustion of a perfect stoichiometric ratio of hydrogen and oxygen gas in the vessel headspace, assuming no venting of pressure / fluid through the ejection port (Adiabatic Isochoric Constant Combustion; AICC) (Lautkaski 2005). In our analysis we estimated a final temperature from an initial ambient temperature (25° C) of the stoichiometric hydrogen / oxygen mixture, and the temperature change based on the enthalpy of combustion of hydrogen and constant volume specific heat of water vapor resulting from the explosion. The maximum pressure was estimated from this temperature value using the ideal gas law and the total number of molecules of water vapor resulting from explosion of the stoichiometric mixture of hydrogen and oxygen initially at 1 atmosphere of pressure. The maximum pressure was then used to estimate the maximum stress in the cylindrical vessel, as the orthogonal sum of the hoop stress and axial stresses. Our estimated maximum stress (29.9 mPa) was then compared to the yield stress of the acrylic (69 mPa), to obtain a safety factor of 2.3, indicating no risk of explosion of the vessel under the above conservative assumptions.

9. CONCLUSION

Sample acquisition, concentration and detection of bacterial contaminants was achieved in less than 2 hours without a specialized laboratory facility or traditional enrichment methods by a custom designed portable, automated electroflotation EF system (Figure 35). The EF system was capable of concentrating hundreds of mL (380 mL) containing 10^2 CFU/mL *E. coli* into 1 mL containing approximately 10^4 – 10^5 CFU/mL. This technology is ideal to support and enhance sensitive detection of bacterial contaminants by portable molecular diagnostics especially in point-of-care testing. All processes presented in this research can be performed during field testing including DNA extraction (crude cell lysis) and removal of LAMP inhibitors. The degree to which the EF system was capable of concentrating bacteria dispersed in media was measured indirectly, by observing changes in detection rates of a LAMP assay. Identifying the limit of detection of the LAMP assay without EF treatment allowed us to infer that if reliable detection was achieved, the EF system must concentrate the bacteria levels above this limit. The designed LAMP assay could detect dispersed *E. coli* present in quantities of 10^4 CFU/mL and 10^5 CFU/mL at a rate of ~50% and 100% respectively. Optimizing surfactant (pluronic F-68) and flocculant (chitosan) concentrations eventually allowed us to reliably detect bacterial quantities of 10^2 CFU/mL at an average rate of 96.3%-100%. The EF system met the detection rate (~95%) required for testing high consequence pathogens at the tested levels, and detection limits may be improved more through scale up of the original sample, reduction in the recovered fraction volume, or for other assays with lower detection limits than the one we used for demonstration in this research (Kubota and Jenkins 2015a).

.

Figure 35. Image of Electroflotation System. For testing the efficacy of electroflotation treatment for point-of-care sample preparation we designed a self-contained battery powered EF cartridge interfaced wirelessly to an Android app.

To my knowledge, the proposed technology is novel and addresses needs of federal agencies such the EPA, which has ongoing research initiatives aimed towards innovative approaches to separate bacteria, viruses and parasites from large volumes of water, up to 1600 liters. The EF system demonstrates potential to be adapted into current or new state or federal water, food, agriculture or aquaculture testing methodologies. We have ongoing collaborations with the Water Resources Research Center at the University of Hawai‘i at Mānoa aimed to integrate these technologies to detect microbial communities in Honolulu’s water supplies, to evaluate contamination risks and to aid resource management to make informed decisions during disasters like hurricanes, flooding, and sewage contamination (data not shown). Many pacific islands like Guam and Samoa face similar water quality challenges and would benefit from

knowledge generated in Hawaii and this research. Portable biotechnology has broad applications in Hawai‘i’s growing aquaculture industry and sustainable farming infrastructure, especially in the context of expanded testing requirements under the Food Safety Modernization Act.

REFERENCE**S:**

111th Congress. 2011. An Act To amend the Federal Food, Drug, and Cosmetic Act with respect to the safety of the food supply. Pharm. Law Desk Ref.:111–353.

Abdel-Hamid I, Ivnitski D, Atanasov P, Wilkins E. 1999. Highly sensitive flow-injection immunoassay system for rapid detection of bacteria. Anal. Chim. Acta 399:99–108.

Alam R, Shang JQ. 2016. Journal of Water Process Engineering Electrochemical model of electro-flotation. J. Water Process Eng. 12:78–88.

Almutairi Z, Ren CL, Simon L. 2012. Evaluation of polydimethylsiloxane (PDMS) surface modification approaches for microfluidic applications. Colloids Surfaces A Physicochem. Eng. Asp. 415:406–412.

Angelopoulos M. 2001. Conducting polymers in microelectronics Conjugated polymers in the nondoped and. Current 45:57–75.

Ballantyne A. Advanced Surface Protection for Improved Reliability PCB Systems (ASPIS).
Barany S, Szepesszentgyörgyi A. 2004. Flocculation of cellular suspensions by polyelectrolytes. Adv. Colloid Interface Sci. 111:117–29.

Bhattacharya S, Datta A, Berg JM, Gangopadhyay S. 2005. Studies on surface wettability of poly(dimethyl) siloxane (PDMS) and glass under oxygen-plasma treatment and correlation with bond strength. J. Microelectromechanical Syst. 14:590–597.

Bhattacharya S, Gao Y, Korampally V, Othman MT, Grant SA, Gangopadhyay K, Gangopadhyay S. 2007. Mechanics of plasma exposed spin-on-glass (SOG) and polydimethyl siloxane (PDMS) surfaces and their impact on bond strength. Appl. Surf. Sci. 253:4220–4225.

Bodas D, Khan-Malek C. 2006. Formation of more stable hydrophilic surfaces of PDMS by plasma and chemical treatments. Microelectron. Eng. 83:1277–1279.

Bodas D, Khan-Malek C. 2007. Hydrophilization and hydrophobic recovery of PDMS by oxygen plasma and chemical treatment-An SEM investigation. Sensors Actuators, B Chem. 123:368–373.

Bouazaze H, Cattarin S, Huet F, Musiani M, Nogueira RP. 2006. Electrochemical noise study of the effect of electrode surface wetting on the evolution of electrolytic hydrogen bubbles. J. Electroanal. Chem. 597:60–68.

Breslin CB, Fenelon AM, Conroy KG. 2005. Surface engineering: corrosion protection using conducting polymers. Mater. Des. 26:233–237.

Bui Q V., Nam ND, Choi DH, Lee JB, Lee CY, Kar A, Kim JG, Jung SB. 2010. Corrosion protection of ENIG surface finishing using electrochemical methods. Mater. Res. Bull. 45:305–

308.

Cao W, Easley CJ, Ferrance JP, Landers JP. 2006. Chitosan as a polymer for pH-induced DNA capture in a totally aqueous system. Anal. Chem. 78:7222–7228.

Chandler DP, Brown J, Call DR, Wunschel S, Grate JW, Holman DA, Olson L, Stottlemyre MS, Bruckner-Lea CJ. 2001. Automated immunomagnetic separation and microarray detection of E. coli O157:H7 from poultry carcass rinse. Int. J. Food Microbiol. 70:143–154.

Chen G. 2004. Electrochemical technologies in wastewater treatment. Sep. Purif. Technol. 38:11–41.

Chisti Y. 2000. Animal-cell damage in sparged bioreactors. Trends Biotechnol. 18:420–432.

Chung YC, Yeh JY, Tsai CF. 2011. Antibacterial characteristics and activity of water-soluble chitosan derivatives prepared by the Maillard reaction. Molecules 16:8504–8514.

Duby P. 1993. The history of progress in dimensionally stable anodes. JOM 45:41–43.

Elias CB, Desai RB, Patole MS, Joshi JB, Mashelkar RA. 1995. Turbulent shear stress - effect on mammalian cell culture and measurement using laser doppler anemometer. Chem. Eng. 50:2431–2440.

Fan W, Wu X, Ding B, Gao J, Cai Z, Zhang W, Yin D, Wang X, Zhu Q, Liu J, et al. 2012. Degradable gene delivery systems based on Pluronics-modified low-molecular-weight polyethylenimine: Preparation, characterization, intracellular trafficking, and cellular distribution. Int. J. Nanomedicine 7:1127–1138.

Farías T, de Ménorval LC, Zajac J, Rivera A. 2009. Solubilization of drugs by cationic surfactants micelles: Conductivity and 1H NMR experiments. Colloids Surfaces A Physicochem. Eng. Asp. 345:51–57.

Fu H, Lee D, Lee J, Tong G, Lee S, Kazi A, Nailos M, Ables W, Corporation D. Main Menu Creep Corrosion Failure Analysis on ENIG Printed Circuit Boards Main Menu. :381–386.

Fu Z, Rogelj S, Kieft TL. 2005. Rapid detection of Escherichia coli O157:H7 by immunomagnetic separation and real-time PCR. Int. J. Food Microbiol. 99:47–57.

G. H. 2009. Nucleic Acid Sample Preparation for Downstream Analyses. In: The Federation of European Biochemical Societies Journal. Vol. 28-9624–0. p. 1–171.

Garg S, Wang L, Schenk PM. 2014. Effective harvesting of low surface-hydrophobicity microalgae by froth flotation. Bioresour. Technol. 159:437–441.

Ghernaout D, Benblidia C, Khemici F. 2015. Microalgae removal from Ghrib Dam (Ain Defla, Algeria) water by electroflotation using stainless steel electrodes. Desalin. Water Treat. 54:3328–

3337.

Gonzales LV, Veneu DM, Torem ML. 2012. MEASUREMENT AND ANALYSIS OF MICRO-BUBBLES. :2136–2146.

Gregory J, Barany S. 2011. Adsorption and flocculation by polymers and polymer mixtures. Adv. Colloid Interface Sci. 169:1–12.

Halladay, D., Resnik R. 1963. Physics for Students of Science and Engineering. John Wiley and Sons.

Halldorsson S, Lucumi E, Gómez-Sjöberg R, Fleming RMT. 2015. Advantages and challenges of microfluidic cell culture in polydimethylsiloxane devices. Biosens. Bioelectron. 63:218–231.

Hemmilä S, Cauich-Rodríguez J V., Kreutzer J, Kallio P. 2012. Rapid, simple, and cost-effective treatments to achieve long-term hydrophilic PDMS surfaces. Appl. Surf. Sci. 258:9864–9875.

HOFFMANN S, BATZ MB, MORRIS JG. 2012. Annual Cost of Illness and Quality-Adjusted Life Year Losses in the United States Due to 14 Foodborne Pathogens. J. Food Prot. 75:1292–1302.

Hu S, Ren X, Bachman M, Sims CE, Li GP, Allbritton N. 2002. Surface modification of poly(dimethylsiloxane) microfluidic devices by ultraviolet polymer grafting. Anal. Chem. 74:4117–4123.

Jacobs A, Lafolie F, Herry JM, Debroux M. 2007. Kinetic adhesion of bacterial cells to sand: Cell surface properties and adhesion rate. Colloids Surfaces B Biointerfaces 59:35–45.

Joshi JB, Elias CB, Patole MS. 1996. Role of hydrodynamic shear in the cultivation of animal, plant and microbial cells. Chem. Eng. J. Biochem. Eng. J. 62:121–141.

Karim MN, Graham H, Han B, Cibulskas A. 2008. Flocculation enhanced microfiltration of Escherichia coli lysate. Biochem. Eng. J. 40:512–519.

Khosla A. 2012. Nanoparticle-doped Electrically-conducting Polymers for Flexible Nano-Micro Systems. ECS Interface 21:67–70.

Kong M, Chen XG, Xing K, Park HJ. 2010. Antimicrobial properties of chitosan and mode of action: A state of the art review. Int. J. Food Microbiol. 144:51–63.

Kubota R, Alvarez AM, Su WW, Jenkins DM. 2011. FRET-Based Assimilating Probe for Sequence-Specific Real-Time Monitoring of Loop-Mediated Isothermal Amplification (LAMP). 4:81–100.

Kubota R, Jenkins DM. 2015a. Real-time duplex applications of loop-mediated AMPlification (LAMP) by assimilating probes. Int. J. Mol. Sci. 16:4786–99.

Kubota R, Jenkins DM. 2015b. Real-Time Duplex Applications of Loop-Mediated AMPlification (LAMP) by Assimilating Probes. :4786–4799.

Kurniawati HA, Ismadji S, Liu JC. 2014. Microalgae harvesting by flotation using natural saponin and chitosan. Bioresour. Technol. 166:429–434.

Kyzas G, Matis K. 2014. Flotation of Biological Materials. Processes 2:293–310.
Lautkaski R. 2005. Pressure Rise in Confined Gas Explosions. Vtt.Fi.

Lazarenko E.N., Baran A.A. MY V. 1986. Flotation of bacterial suspensions using cationic flocculants.pdf. Colloid J. USSR 48:493–496.

Lee, H.Y., Barber, C., Minerick AR. 2014. Improving Electrokinetic microdeivce stability by controlling electrolysis bubbles. Electrophoresis 35:1782–1789.

de Leon A, Advincula RC. 2015. Chapter 11 – Conducting Polymers with Superhydrophobic Effects as Anticorrosion Coating. In: Intelligent Coatings for Corrosion Control. p. 409–430.

Liang C, Chu Y, Cheng S, Wu H, Kajiyama T, Kambara H, Zhou G. 2012. Multiplex loop-mediated isothermal amplification detection by sequence-based barcodes coupled with nicking endonuclease-mediated pyrosequencing. Anal. Chem. 84:3758–3763.

Lide DR. 1994. Dissociation Constants, Ionic Conductivities. In: CRC Handbook of Chemistry and Physics. 74th ed. CRC Press. p. 8–47, 5–91.

Lu J, Gerke TL, Buse HY, Ashbolt NJ. 2014. Development of an Escherichia coli K12-specific quantitative polymerase chain reaction assay and DNA isolation suited to biofilms associated with iron drinking water pipe corrosion products. J. Water Health 12:763–771.

Luo C, Meng F, Francis A. 2006. Fabrication and application of silicon-reinforced PDMS masters. Microelectronics J. 37:1036–1046.

Luo Y, Huang B, Wu H, Zare RN. 2006. Controlling electroosmotic flow in poly(dimethylsiloxane) separation channels by means of prepolymer additives. Anal. Chem. 78:4588–4592.

Ma N, Chalmers JJ, Auniņš JG, Zhou W, Xie L. 2004. Quantitative studies of cell-bubble interactions and cell damage at different pluronic F-68 and cell concentrations. Biotechnol. Prog. 20:1183–1191.

Mandal PK, Biswas AK, Choi K, Pal UK. 2011. Methods for Rapid Detection of Foodborne Pathogens: An Overview. Am. J. Food Technol. 6:87–102.

Maron P, Schimann H, Ranjard L, Brothier E, Domenach A, Lensi R, Nazaret S. 2006. Evaluation of quantitative and qualitative recovery of bacterial communities from different soil

types by density gradient centrifugation. 42:65–73.
Martzy R, Kolm C, Brunner K, Mach RL, Krska R, Šinkovec H, Sommer R, Farnleitner AH, Reischer GH. 2017. A loop-mediated isothermal amplification (LAMP) assay for the rapid detection of Enterococcus spp. in water. Water Res. 122:62–69.

Metters JP, Gomez-Mingot M, Iniesta J, Kadara RO, Banks CE. 2013. The fabrication of novel screen printed single-walled carbon nanotube electrodes: Electroanalytical applications. Sensors Actuators B Chem. 177:1043–1052.

Metters JP, Kadara RO, Banks CE. 2012. Electroanalytical properties of screen printed graphite microband electrodes. Sensors Actuators, B Chem. 169:136–143.

Montemayor LC. 2002. Electrically Conductive Silicone Adhesive. SMTA Int. Conf.
Montes-Atenas G, Garcia-Garcia FJ, Mermillod-Blondin R, Montes S. 2010. Effect of suspension chemistry onto voltage drop: Application to electro-flotation. Powder Technol. 204:1–10.

Moscicki A, Sobierajski T, Falat T, Felba J. The post-curing technology for conductivity improvement of low- viscosity electrically conductive adhesives. :2–5.

Mozes, N, Amory, D.E., Leonard, A.J., Rouxhet PG. 1989. Surface Properties of Microbial Cells and Their Role in Adhesion and Flocculation. Colloids and Surfaces 42:313–329.

Murugananthan M, Bhaskar Raju G, Prabhakar S. 2004. Separation of pollutants from tannery effluents by electro flotation. Sep. Purif. Technol. 40:69–75.

Nagai N, Takeuchi M, Kimura T, Oka T. 2003. Existence of optimum space between electrodes on hydrogen production by water electrolysis. Int. J. Hydrogen Energy 28:35–41.

Nagamine K, Hase T, Notomi T. 2002. Accelerated reaction by loop-mediated isothermal amplification using loop primers. Mol. Cell. Probes 16:223–229.

Nguyen A V., Evans GM. 2002. The liquid flow force on a particle in the bubble-particle interaction in flotation. J. Colloid Interface Sci. 246:100–104.

Notomi T, Okayama H, Masubuchi H, Yonekawa T, Watanabe K, Amino N, Hase T. 2000. Loop-mediated isothermal amplification of DNA. Nucleic Acids Res. 28:E63.

Pearson CR, Heng M, Gebert M, Glatz CE. 2004. Zeta potential as a measure of polyelectrolyte flocculation and the effect of polymer dosing conditions on cell removal from fermentation broth. Biotechnol. Bioeng. 87:54–60.

Percino, M. J. and Chapela VM. 2013. Conducting Polymers, in Handbook of Polymer Synthesis, Characterization, and Processing. E. Saldívar-Guerra and E. Vivaldo-Lima, editor. Inc., Hoboken, NJ, USA: John Wiley & Sons.

QIN C, LI H, XIAO Q, LIU Y, ZHU J, DU Y. 2006. Water-solubility of chitosan and its antimicrobial activity. Carbohydr. Polym. 63:367–374.

Rinaudo M. 2006. Chitin and chitosan: Properties and applications. Prog. Polym. Sci. 31:603–632.

Rohwerder M, Michalik A. 2007. Conducting polymers for corrosion protection: What makes the difference between failure and success? Electrochim. Acta 53:1300–1313.

Sahoo PR, Sethy K, Mohapatra S, Panda D. 2016. Loop mediated isothermal amplification: An innovative gene amplification technique for animal diseases. Vet. World 9:465–469.

Salahinejad E, Eslami-Farsani R, Tayebi L. 2017. Corrosion failure analysis of printed circuit boards exposed to H 2 S-containing humid environments. Eng. Fail. Anal. 79:538–546.

Santos DMF, Sequeira CAC, Figueiredo JL. 2013. Hydrogen production by alkaline water electrolysis. Quim. Nova 36:1176–1193.

Scharff RL. 2012. Economic Burden from Health Losses Due to Foodborne Illness in the United States. J. Food Prot. 75:123–131.

Sharma PK, Gibcus MJ, Van Der Mei HC, Busscher HJ. 2005. Influence of fluid shear and microbubbles on bacterial detachment from a surface. Appl. Environ. Microbiol. 71:3668–3673.

Sowana DD, Williams DRG, Dunlop EH, Dally BB, O'Neill BK, Fletcher DF. 2001. Turbulent Shear Stress Effects on Plant Cell Suspension Cultures. Chem. Eng. Res. Des. 79:867–875.

Stevens KA, Jaykus L-AA. 2004. Bacterial separation and concentration from complex sample matrices: a review. Crit. Rev. Microbiol. 30:7–24.

Strand SP, Nordengen T, Ostgaard K. 2002. Efficiency of chitosans applied for flocculation of different bacteria. Water Res. 36:4745–52.

Strand SP, Vandvik MS, Vårum KM, Østgaard K. 2001. Screening of chitosans and conditions for bacterial flocculation. Biomacromolecules 2:126–133.

Strand SP, Vårum KM, Østgaard K. 2003. Interactions between chitosans and bacterial suspensions: Adsorption and flocculation. Colloids Surfaces B Biointerfaces 27:71–81.

Sugimoto M, Morimoto M, Sashiwa H, Saimoto H, Shigemasa Y. 1998. Preparation and characterization of water-soluble chitin and chitosan derivatives. Carbohydr. Polym. 36:49–59.

Švancara I, Vytřas K, Kalcher K, Walcarius A, Wang J. 2009. Carbon Paste Electrodes in Facts, Numbers, and Notes: A Review on the Occasion of the 50-Years Jubilee of Carbon Paste in Electrochemistry and Electroanalysis. Electroanalysis 21:7–28.

Szpyrkowicz L. 2005. Hydrodynamic effects on the performance of electro-coagulation/electro-flotation for the removal of dyes from textile wastewater. Ind. Eng. Chem. Res. 44:7844–7853.
Taylor P, Ghosh M, Ganguli A, Pathak S. 2009. Application of a novel biopolymer for removal of Salmonella from poultry wastewater.

Teh CSJ, Chua KH, Lim YAL, Lee SC, Thong KL. 2014. Loop-mediated isothermal amplification assay for detection of generic and verocytotoxin-producing escherichia coli among indigenous individuals in malaysia. Sci. World J. 2014.

Tharmalingam T, Ghebeh H, Wuerz T, Butler M. 2008. Pluronic enhances the robustness and reduces the cell attachment of mammalian cells. Mol. Biotechnol. 39:167–177.

Thatcher SA. 2015. DNA/RNA preparation for molecular detection. Clin. Chem. 61:89–99.

Walls PLL, Bird JC, Bourouiba L. 2014. Moving with bubbles: a review of the interactions between bubbles and the microorganisms that surround them. Integr. Comp. Biol. 54:1014–1025.

Wang H, Turechek WW. 2016. A loop-mediated isothermal amplification assay and sample preparation procedure for sensitive detection of Xanthomonas fragariae in strawberry. PLoS One 11:1–21.

Wilson IG, Wilson I a NG. 1997. Inhibition and Facilitation of Nucleic Acid Amplification Inhibition and Facilitation of Nucleic Acid Amplification. 63:3741–3751.

Yang Z, Yuan B, Huang X, Zhou J, Cai J, Yang H, Li A, Cheng R. 2012. Evaluation of the flocculation performance of carboxymethyl chitosan-graft-polyacrylamide, a novel amphoteric chemically bonded composite flocculant. Water Res. 46:107–114.

You DJ, Geshell KJ, Yoon JY. 2011. Direct and sensitive detection of foodborne pathogens within fresh produce samples using a field-deployable handheld device. Biosens. Bioelectron. 28:399–406.

Zarras P, Anderson N, Webber C, Irvin DJ, Irvin JA, Guenthner A, Stenger-Smith JD. 2003. Progress in using conductive polymers as corrosion-inhibiting coatings. Radiat. Phys. Chem. 68:387–394.

Zhang J, Liang Z, Hreid T, Yuan Z. 2012. RSC Advances Fabrication and investigation of a new copper-doped screen-printable carbon paste ’ s conductive mechanism by AFM {. :4787–4791.

Zhao LH, Lee J, Sen PN. 2012. Long-term retention of hydrophilic behavior of plasma treated polydimethylsiloxane (PDMS) surfaces stored under water and Luria-Bertani broth. Sensors Actuators, A Phys. 181:33–42.

Zhao Y, Gu S, Gong K, Zheng J, Wang J, Yan Y. 2017. Iodine Redox-Mediated Electrolysis for Energy-Efficient Chlorine Regeneration from Gaseous HCl. J. Electrochem. Soc. 164:E138–E143.

Zhou W, Gao L, Cheng W, Chen L, Wang J, Wang H, Zhang W, Liu T. 2016. Electro- fl otation of Chlorella sp . assisted with fl occulation by chitosan. ALGAL 18:7–14.

Zimmerman WB, Tesa V, Butler S, Bandulasena HCH. 2008. Microbubble Generation. Recent Patents Eng. 2:1–8.

Zita A, Hermansson M. 1997. Effects of bacterial cell surface structures and hydrophobicity on attachment to activated sludge flocs. Appl. Environental Microbiol. 63:1168–1170.

APPENDIX

Strains	Source	LAMP *in silico*	Query cover %
Acinetobacter baumannii	ATCC 19606	-	0
Aeromonas hydrophila	ATCC 7966	-	56
Aeromonas caviae	ATCC 15468	-	8-15
Bacillus cereus	ATCC 10876	-	0
Burkholderia cepacia	ATCC 25416	-	40
Campylobacter jejuni	ATCC 33560	-	0
Citrobacter freundii	ATCC 8090	-	6-7
Enterobacter aerogenes	ATCC 13048	-	53
Enterobacter cloacae	ATCC 13047	-	0
Enterococcus faecalis	ATCC 19433	-	0
Enterococcus faecium	ATCC 19434	-	0
Klebsiella oxytoca	ATCC 13182	-	60
Klebsiella pneumoniae	ATCC 25955	-	0
Lactobacillus acidophilus	ATCC 4796	-	0
Listeria monocytogenes	Scott A	-	0
Micrococcus luteus	ATCC 4698	-	0
Proteus mirabilis	ATCC 29906	-	0
Proteus vulgaris	ATCC 29905	-	28
Pseudomonas aeruginosa	ATCC 14886	-	0
Salmonella enterica		-	56
Serratia marcescens	ATCC 13880	-	6-7
Shigella sonnei		-	34
Staphylococcus aureus	ATCC 51811	-	0
Staphylococcus aureus	ATCC BAA-39	-	0
Streptococcus pyogenes	ATCC 10782	-	7
Yersinia enterocolitica		-	13-43

Table A1. Specificity tests of modified LAMP primer to non-*E. coli* strains. *in silico* results with respective query coverage (%) to primer set EcolC 3109_1. Query coverage is calculated by considering the percentage of the input sequence (query ie. Primer sequences) overlapping the entire genome of the non-*E. coli* strains retrieved from the NCBI database.

Strains	Accession	Identities %	Mismatch %					
			F3	B3	FIP	BIP	LF	LB
E. coli ATCC 25922	CP009072.1	100	0	0	0	0	0	0
E. coli NU14	CP019777.1	100	0	0	0	0	0	0
E. coli UPEC 26-1	CP016497.1	100	0	0	0	0	0	0
E. coli K15KW01	CP016358.1	100	0	0	0	0	0	0
E. coli ECONIH2	CP014667.1	100	0	0	0	0	0	0
E. coli SF-166	CP012633.1	100	0	0	0	0	0	0
E. coli SF-173	CP012631.1	100	0	0	0	0	0	0
E. coli SF-088	CP012635.1	100	0	0	0	0	0	0
E. coli SF-468	CP012625.1	100	0	0	0	0	0	0
E. coli NMEC O187	CP007275.1	100	0	0	0	0	0	0
E. coli APEC O18	CP006830.1	100	0	0	0	0	0	0
E. coli RS218	CP007149.1	100	0	0	0	0	0	0
E. coli APEC IMT5155	CP005930.1	100	0	0	0	0	0	0
E. coli Nissle 1917	CP007799.1	100	0	0	0	0	0	0
E. coli PMV-1	HG428755.1	100	0	0	0	0	0	0
E. coli clone D i14	CP002212.1	100	0	0	0	0	0	0
E. coli clone D i2	CP002211.1	100	0	0	0	0	0	0
E. coli UM146	CP002167.1	100	0	0	0	0	0	0
E. coli ABU 83972	CP001671.1	100	0	0	0	0	0	0
E. coli IHE3034	CP001969.1	100	0	0	0	0	0	0
E. coli S88 Chromosome	CU928161.2	100	0	0	0	0	0	0
E. coli APEC O1	CP000468.1	100	0	0	0	0	0	0
E. coli 536	CP000247.1	100	0	0	0	0	0	0
E. coli UTI89	CP000243.1	100	0	0	0	0	0	0
E. coli CFT073	AE014075.1	100	0	0	0	0	0	0
E. coli isolate NRZ14408	LT599825.1	99	0	0	0	0	11	0
E. coli AR_0061	CP020058.1	97	0	0	7	0	11	0
E. coli M18	CP010219.1	97	0	0	7	0	11	0
E. coli M10	CP010200.1	97	0	0	7	0	11	0
E. coli M9	CP010196.1	97	0	0	7	0	11	0
E. coli ATCC 8739	CP000946.1	97	0	0	7	0	11	0
E. coli Ecol_AZ147	CP018995.1	97	0	0	7	0	11	0
E. coli BLR(DE3)	CP020368.1	96	0	0	7	2	11	0
E. coli HB-Coli0	CP020933.1	96	0	0	7	2	11	0
E. coli AR_0069	CP020055.1	96	0	0	7	2	11	0
E. coli M8	CP019953.1	96	0	0	7	2	11	0
E. coli Ecol_316	CP018957.1	96	0	0	7	2	11	0
E. coli AR_0118	CP020048.1	96	0	0	7	2	11	0
E. coli 13E0767	CP020107.1	96	0	0	7	2	11	0
E. coli 13E0780	CP020106.1	96	0	0	7	2	11	0

E. coli 13E0725	CP020092.1	96	0	0	7	2	11	0
E. coli S21	CP010230.1	96	0	0	7	2	11	0
E. coli Ecol_517	CP018965.1	96	0	0	7	2	11	0
E. coli Ecol_224	CP018948.1	96	0	0	7	2	11	0
E. coli WCHEC1613	CP019213.1	96	0	0	7	2	11	0
E. coli S56	CP010242.1	96	0	0	7	2	11	0
E. coli S50	CP010238.1	96	0	0	7	2	11	0
E. coli S42	CP010236.1	96	0	0	7	2	11	0
E. coli S30	CP010231.1	96	0	0	7	5	11	0
E. coli Ecol_545	CP018976.1	96	0	0	7	5	11	0
E. coli K12, W3110	AP009048.1	96	5	0	7	2	11	0
E. coli K12, MG1655	NZ_APIN01000002.1	96	5	0	7	2	11	0
E. coli K12, DH1	CP001637.1	96	5	0	7	2	11	0
E. coli 2016C-3936C1	CP018770.2	96	0	0	10	2	11	0
E. coli DSM 103246	CP019944.1	96	0	0	10	2	11	0
E. coli MDR_56	CP019903.1	95	0	0	10	2	11	5
E. coli DNA 20Ec-P-124	AP017610.1	95	0	0	10	2	11	5
E. coli Ecol_881	CP019029.1	95	0	0	10	2	11	5

Table A2. *E. coli* strains % identity match with modified primer (glycerate kinase gene region and primer set EcolC 3109_1). Percent match is calculated using only the homologous regions of the primer binding sites and not the entire gene region. Mismatch percent is calculated based on the proportion of mismatched base pairs for each primer individually.